Quaternary International xxx (xxxx) xxx

Contents lists available at ScienceDirect

Quaternary International

journal homepage: www.elsevier.com/locate/quaint

Forward and inverse methods for extracting climate and diet information from stable isotope profiles in proboscidean molars

Kevin T. Uno [a,*,1], Daniel C. Fisher [b,c], George Wittemyer [d,e], Iain Douglas-Hamilton [e,f], Nancy Carpenter [g], Patrick Omondi [h], Thure E. Cerling [a,i]

[a] Department of Geology and Geophysics, University of Utah, Salt Lake City, UT, 84112, USA
[b] Museum of Paleontology, University of Michigan, Ann Arbor, MI, 48109, USA
[c] Department of Earth and Environmental Sciences, University of Michigan, Ann Arbor, MI, 48109, USA
[d] Department of Fish, Wildlife and Conservation Biology, Colorado State University, Fort Collins, CO, 80523, USA
[e] Save the Elephants, Nairobi, 00200, Kenya
[f] Department of Zoology, Oxford University, Oxford, OX1 3PS, United Kingdom
[g] Utah's Hogle Zoo, Salt Lake City, UT, 84108, USA
[h] Kenya Wildlife Services, Nairobi, Kenya
[i] Department of Biology, University of Utah, Salt Lake City, UT, 84112, USA

ARTICLE INFO

Keywords:
Intratooth profile
Stable isotope
Proboscidean
Microsampling
Enamel maturation
Paleecology

ABSTRACT

Intratooth stable isotope profiles in enamel provide time series of dietary and environmental information that if correctly interpreted, serve as archives of seasonal variability in past environments. A major challenge in interpreting these profiles arises from time averaging imparted by enamel mineralization and developmental geometry, whereby the primary ($\delta^{13}C$ or $\delta^{18}O$) input signal is attenuated and shifted, which can potentially lead to incorrect interpretations of the magnitude or frequency of seasonal variability. Several forward and inverse models have been developed to reconstruct the primary input signal from intratooth profiles in continuously growing teeth. Here the models developed by Passey and Cerling (2002) and Passey et al. (2005) are extended to molars of Elephantinae, which grow over a long but finite interval of time. Proboscidean molars are particularly attractive for intratooth profiles because they may contain a decade or more of information and they are often well preserved in the fossil record because of their thick enamel and large size.

Forward model parameters are established using histological analysis of molar thin sections of extant African elephants (*Loxodonta africana*) and a mammoth (*Mammuthus columbi*) and by micro-CT analysis of *L. africana* molar plates. The density of immature enamel is about 65% of the final density of mature enamel. The appositional length varies from approximately 35 to 55 mm, and the maturation length is about 70 mm. Histological methods are used to determine crown formation time (CFT) in elephant and mammoth molar plates. CFT for the elephant and mammoth molar plates studied in thin section are about 5–6 years and 11 years, which translate to mean growth rates of about 21 mm/year and 16 mm/year, respectively.

Coeval molar and tusk profiles from a zoo elephant are compared. The tusk isotope profile serves as a proxy for the primary input signal, and thus provides an opportunity to evaluate the forward and inverse models. The results from the zoo elephant profiles demonstrate that the inverse model accurately reconstructs the amplitude and overall structure of the primary input signal. Inverse model results of mammoth molar profiles show double the range of $\delta^{13}C$ in measured enamel profiles. Inversion model results illustrate that improved reconstruction of the primary input signal can lead to more accurate interpretations of the seasonal variability of diet and body water and by extension, vegetation and precipitation in past environments.

* Corresponding author.
E-mail address: kevinuno@ldeo.columbia.edu (K.T. Uno).
[1] Current address is Lamont-Doherty Earth Observatory of Columbia University, Palisades, NY, 10964.

https://doi.org/10.1016/j.quaint.2020.06.030
Received 15 December 2019; Received in revised form 18 May 2020; Accepted 19 June 2020
Available online 26 July 2020

1. Introduction

Carbon and oxygen stable isotope ratios in mammalian herbivore teeth record information about an organism's diet, life history, physiology, and environment. A tooth sampled serially along its growth axis provides a stable isotope profile that serves as an isotopic time-series over the period in which it formed, as was first shown in dentin by Koch et al. (1989) and in enamel by Fricke and O'Neil (1996). Since these pioneering studies on intratooth stable isotope profiles, numerous other studies have employed this method to study a wide variety of aspects of seasonality in herbivore ecology that include seasonal diet change (Metcalfe et al., 2011; Uno and Bibi, 2020, *accepted*), past and modern migration patterns (Koch et al., 1998; Tornero et al., 2018), prehistoric herding strategies (Balasse et al., 2002), and seasons of birth (Balasse et al., 2003; Frémondeau et al., 2012) and death (e.g., Koch et al., 1989). Oxygen isotope profiles in tooth enamel have been used to investigate changes in seasonality of climate (Blumenthal et al., 2019; Fricke et al., 1998; Koch et al., 1989; Uno and Bibi, 2020, *accepted*) and changes in paleoelevation over tectonic timescales (Dettman et al., 2001; Kohn et al., 2002).

With the exception of a handful of studies on late Pleistocene proboscidean tusks and molar dentin (e.g., Koch et al., 1989; Rountrey et al., 2012; Rountrey et al., 2007), nearly all mammalian intratooth isotope profiles come from fossil enamel rather than dentin due to the resistance of the former and susceptibility of the latter to diagenetic alteration of the primary isotope signature (Lee-Thorp and dan der Merwe, 1987; Schoeninger and DeNiro, 1982; Wang and Cerling, 1994). Enamel apatite is less susceptible to diagenesis due to its larger crystal size and its lower organic content (<1%) compared to dentin (~20%) (Ayliffe et al., 1994; Elliott, 2002). Although enamel is generally the only fossil material suitable for stable isotope analysis, there is a significant drawback to choosing it over tooth dentin for generating isotope profiles. The prolonged enamel maturation phase and the sampling geometry both lead to attenuation and shifting of the primary input signal recorded in the tooth (Balasse, 2003; Passey and Cerling, 2002).

Enamel formation can be broadly described as occurring in two phases, secretion and maturation, and it proceeds from the apex toward the cervix of the tooth crown (e.g., Hiller et al., 1975; Moss-Salentijn et al., 1997; Suga, 1982), although synchrotron and elemental analyses have elucidated complexities to this process (Green et al., 2017; Trayler and Kohn, 2017). New enamel is deposited on the appositional surface, which is oriented at a low oblique angle to the enamel dentin junction (EDJ). The length of the appositional surface, or appositional length (l_a), is relatively constant in teeth such as hippo canines and rodent incisors, but histological and radiographic data indicate variable l_a in caprine (Zazzo et al., 2010, 2012), bovine (Balasse, 2002; Zazzo et al., 2005), and equine (Hoppe et al., 2004) molars. The addition of each new enamel layer to a developing tooth can be viewed as occurring in a discrete time interval during the secretory phase of enamel formation. In this phase, apatite crystallites are seeded in an organic-rich matrix. As a result, initial enamel density is only a fraction of its final density (e.g., Passey and Cerling, 2002). The organic matter and water are required during matrix deposition and maturation of enamel. Ameloblast cells and the protein amelogenin facilitate mineralization of hydroxylapatite, and body water provides essential ions (Ca^{2+}, PO_4^{3-}, OH^-, and CO_3^{2-}) in solution. During the maturation phase, enamel becomes progressively denser as organic material and body water are replaced with apatite. The maturation process leads to damping of the primary isotopic input signal recorded during the secretory phase as incremental addition of carbon and oxygen (as carbonate ions) occurs throughout the maturation phase.

Sampling also leads to attenuation and temporal shifting in isotope profiles. The conventional sampling method involves drilling a ~1 mm wide path normal to the growth axis of the tooth. The more deeply the drilling path penetrates the enamel, the more time averaging there is as more layers of enamel (e.g., time slices) are combined in the sample. Thus, the main challenge of generating isotope profiles and interpreting the data is that the combined effects of maturation and sampling geometry can attenuate and shift the primary input signal so that the measured isotopic data can give misleading patterns of variability and seasonality (Passey and Cerling, 2002, 2004; Zazzo et al., 2005).

Changes to sampling protocol (e.g., size, geometry, and location) and mathematical modeling are the two main approaches that have been developed in an effort to reconstruct the primary isotopic input signal from measured profile data. The first approach, modification of sampling geometry, principally addresses the time-averaging effects due to sampling. Zazzo et al. (2005) present modeled results from bovine enamel using the forward model of Passey and Cerling (2002) where conventional sampling, sampling parallel to the appositional surface, and sampling the innermost enamel layer are explored. An important result of the modeling was that conventional sampling could produce a sinusoidal profile from nonsinusoidal inputs (fig. 7b of Zazzo et al., 2005), which in fossil teeth would lead to incorrect interpretations of seasonality in past environments. Passey and Cerling (fig. 6 and 2002) show that varying drilling depth using conventional sampling geometry induces temporal shift, but has no effect on isotopic variation.

Several studies have proposed sampling the innermost (10–20 μm) enamel (Balasse, 2003; Blumenthal et al., 2014; Metcalfe et al., 2011; Tafforeau et al., 2007; Zazzo et al., 2005) because the initial enamel density as a proportion of the density of fully mature enamel is higher at the EDJ than in the rest of the enamel (Suga, 1989; Tafforeau et al., 2007). Given the extremely narrow width of this enamel, the method presents limited options for sampling and analysis. Zazzo et al. (2005) demonstrate that isotope profiles can be micromilled at ~20 μm thicknesses from the outer enamel surface to the EDJ, but the overall precision (±100 μm) in drill bit location is five to ten times lower than the desired sample interval. This means there is a high probability that the micromilling method would result in either incorporating adjacent dentin (i.e., over-drilling) or not completely drilling through the entire layer of inner enamel (i.e., under-drilling). An alternative method for targeting the innermost enamel is to drill from the underside of the enamel (Metcalfe et al., 2011), but this is a particularly invasive method that requires completely separating enamel from dentin at the EDJ, which may be quite labor intensive (or unfeasible) for many types of teeth. Widga et al. (2020) developed a method to target innermost enamel in proboscideans building on that of Metcalfe et al. (2011) that instead approaches the innermost 100 μm of enamel via microdrilling from the outer enamel surface. Recovery of the innermost enamel is achieved through wet milling, whereby the water (and entrained enamel powder) is recovered, dried and analyzed untreated in small masses (~150 μg).

Another option for obtaining stable isotope profiles from the inner enamel layer is secondary ion mass spectrometry (SIMS). SIMS can achieve the spatial resolution required (<20 μm), but the number of SIMS instruments available represents only a small fraction of the isotope ratio mass spectrometers (IRMS) available, and thus is currently time and cost prohibitive. SIMS also requires a polished cross section of the enamel, and this may not be feasible for all specimens, especially those belonging to museum collections. Another issue that arises when solely targeting the innermost enamel is that the initial density of the immature enamel must be determined for accurate interpretation of profile data. To date, the only method capable of measuring density at this scale is X-ray synchrotron microtomography (Green et al., 2017; Tafforeau et al., 2007). Accessibility to X-ray synchrotron microtomography facilities is very limited and can be cost prohibitive.

The second approach to recovering the primary carbon or oxygen input signal is through the development of forward and inverse models that consider how stable isotopes are incorporated into developing enamel. Passey and Cerling (2002) proposed a forward model that accounts for the maturation period, geometry of enamel formation, and sampling depth. The main parameters input into the model are initial density as a fraction of the final enamel density (f_i), the length of apposition (l_a), maturation length (l_m), sampling length (Δx), and

sampling depth (Δz) (Fig. 1). The two length parameters (l_m and l_a) are treated as constant, as the model was developed for continuously growing teeth. Using the forward model equations developed in Passey and Cerling (2002) as an operator term **A**, Passey et al. (2005) developed an inverse model whereby inversion of the linear system **Am** = **d**, where **d** is measured profile data, yields **m**, the estimated primary input signal (Fig. S1). More recently, Green and colleagues have developed Bayesian forward and inverse models using x-ray microtomography, tooth dicing (2D sampling) and a Markov Chain Monte Carlo approach for sheep molars (Green et al., 2017, 2018a). These models deal particularly well with ungulate teeth where maturation geometry is not parallel to the developmental geometry and is instead best characterized as a diffusive process (Green et al., 2017).

Stable isotope profiles from teeth that form over multiple years provide an opportunity to investigate terrestrial paleoenvironments at unprecedented resolution and can give insight into seasonal variations in diet and climate. Combined use of forward and inverse models is currently the only method that accounts for time averaging from both the enamel mineralization process and sampling. If the input parameters f_i, l_a, and l_m, can be determined, then inversion of the measured data **d** can provide a reliable estimate of the primary isotopic input signals, which in turn give information about an animal's diet and physiology and about the environment in which it lived. Application of inverse methods to isotope profiles from hypsodont proboscidean molars is an unexplored proxy of seasonality of diet and climate in terrestrial ecosystems throughout the late Neogene. Proboscidean molars are attractive because a single plate (Fig. 2) may contain up to a decade of information (Dirks et al., 2012; Uno et al., 2013), and due to their large size and thick enamel, they are often well preserved in the fossil record.

In this study, forward model parameters (f_i, l_a, and l_m) for the Passey and Cerling model (2002) are determined to describe enamel formation in elephant molars. Parameters f_i and l_m are determined using micro-computed tomography (μ-CT) and l_a is measured on developing plates and in thin sections. Growth rates of individual plates are evaluated using two independent methods, bomb-curve ^{14}C dating and histological analysis of molar thin sections. The forward model is tested by comparing coeval high-resolution tusk data with the molar isotope profiles. The forward model was developed using an evergrowing tooth (i.e., a hippopotamus canine) as a model for enamel growth and geometry, and it treats l_a and l_m as constant. It also assumes that mineralization proceeds at a constant (linear) rate over the maturation phase. Evaluation of the forward model suggests it works satisfactorily for elephant molar plates. Application of the inversion methods developed by Passey et al. (2005) yields an estimated primary input signal that is similar in amplitude and structure to the known input signal from the ivory (tusk dentin) isotope profile. The inverse model is also applied to isotope profiles from molars of a wild African elephant and two Pleistocene fossil mammoths.

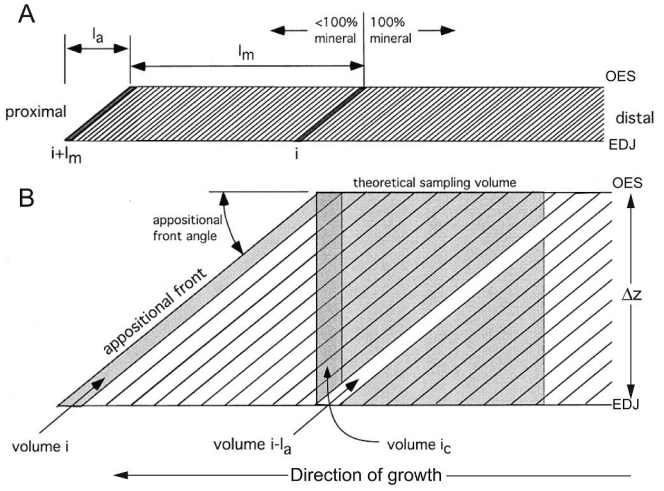

Fig. 1. Schematic of an enamel cross-section illustrating enamel formation and model parameters described in equations (3) to (5) in the Supplementary Information (SI). Only enamel is shown, the EDJ is at the bottom and the outer enamel surface (OES) at the top of each schematic. Enamel is forming from right to left. a) Model parameters l_a and l_m are shown. Volume i is in the final stage of maturation whereas volume i + l_m is the most recently formed volume in the secretory phase with density f_i. b) Volume i is also shown here, as is volume i_c, a column described in SI equation (4). A theoretical sampling volume described in SI equation (5) is comprised of n columns of dimension i_c, and is shown here with a depth (Δz) through the full enamel thickness by the shaded square. From Passey and Cerling (2002).

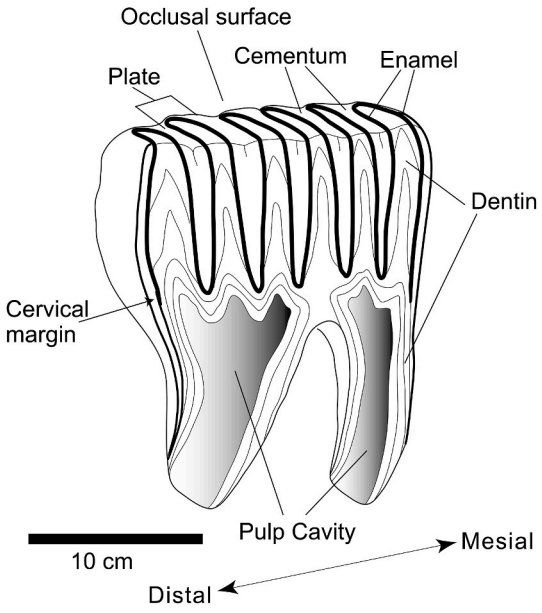

Fig. 2. Schematic drawing of a fully-formed proboscidean molar with a worn occlusal surface. The molar comprises six plates cemented together. Each enamel-covered plate has a dentin interior and is joined to adjacent plates by cementum. Modified from Fisher and Fox (2007).

2. Background and materials

Molars and tusks from four extant African elephants and two *Mammuthus columbi* molars were used in the study. For two of the elephants, Misha and R37, some tusk and molar material has been previously analyzed (Uno et al., 2020; Uno et al., 2013). Misha was captured in South Africa at an estimated age of 1 year old in 1982 and later transferred to the Happy Hollow Zoo in San Jose, California. She was transferred again in August of 1983 to Marine World Africa in nearby Redwood Shores, CA and then sometime in 1986 moved once more to Six Flags Discovery Kingdom in Vallejo, CA where she remained for nearly 20 years. On April 22, 2005, Misha made her final move, from California to Utah's Hogle Zoo in Salt Lake City. On September 9, 2009 Misha was euthanized due to rapidly declining health at an age of approximately 27 years old. The Hogle Zoo agreed to loan one tusk and several molars to the University of Utah for study. Data come from Misha's tusk dentin and lower right third molar (m3), although additional molars (lower left m3) and additional loose plates that were not able to be assigned to specific molars were also loaned for study. We use the general nomenclature for mammal molars rather than the Laws nomenclature (molars 1 through 6), whereby the term m3 referred to in this study is the last molar (Laws' m6) to form (Laws, 1966).

R37 was a female elephant from Kenya who died on September 26, 2006. R37 was the matriarch of an elephant family unit called the Swahilis. The Swahilis inhabit the Samburu, Buffalo Springs, and Shaba

National Reserves and surrounding area in northern Kenya (Wittemyer, 2001; Uno et al., 2020). Using the tooth wear age criteria established by Laws (1966) and refined by Lee et al. (2012), the estimated age of R37 at death was 53 ± 5 years old. A tusk, molars and tail hairs from R37 were imported using a permit granted by the Convention on International Trade of Endangered Species (CITES) and the US Fish and Wildlife Service. Using data from GPS collars and field observations, Wittemyer and Getz (2007) determined the rank of 20 family unit matriarchs in and around the Reserves; R37's rank of 13th classified her as mid-low in the social hierarchy and as a result, she had a larger home range than higher ranking matriarchs (549 km^2).

Other molars come from elephants that lived in and around Tsavo National Park (TNP) and Samburu National Reserve (SNR), Kenya. For the individual from TNP, TE-95, there are two molars, a lower right m2 (or possibly an m1) and a lower right m3 (or possibly an m2). Based on the molar size, we presume TE-95 was a male. Bomb-curve ^{14}C dating of the m3 indicates 1964 as the year of death (Uno et al., 2013). The molar from the SNR elephant is K07-M53.95A (hereafter K07-M53), which is an unerupted lower m1 (or possibly m2) that was removed from the mandibular crypt. The estimated year of death of K07-M53 is 2006.

Each molar or tusk from the four different elephants possesses unique attributes that contribute to the study. Extensive background information on R37 and the ability to work on both the tusk and molar provide an opportunity to compare how diet and climate signals are recorded in the two tissues, tusk dentin and molar enamel (Uno et al., 2020). Misha's tusk and molar provide a similar opportunity to compare isotope profiles from the two tissues, but with greater constraint on the isotope ratios in the tissues formed during her time in Utah. A section of her developing molar is used for studying enamel formation. In both cases, the tusk dentin profiles serve as primary input signals for diet and body water with which to validate the forward and inverse models (Fig. S1).

The TE-95 molars formed from the mid-1950s to the mid-1960s when the pulse of anthropogenic ^{14}C was produced in the atmosphere, providing an excellent opportunity to determine growth rates using bomb-curve ^{14}C age-dating techniques developed in Uno et al. (2013). The developing molar from K07-M53 is used to study enamel maturation using micro-CT.

Two late Pleistocene mammoth (*Mammuthus columbi*) molars are also used in this study. Specimen LACM-47129 is from the Rancholabrean locality of Costeau Pit in Orange County, CA (Miller, 1971). The specimen consists of the three most mesial plates of an unerupted molar. The other specimen, IMNH-40368, is a ~10 cm long fragment of an enamel plate spalled off from the posterior side of a molar plate. The specimen comes from layer "E" at the American Falls fossil site in Idaho, and is also of Rancholabrean age. Based on a K/Ar age date on the overlying Cedar Butte basalt of 72 ± 14 ka, the age of layer E is approximately 125 ka (Pinsof, 1992; Scott et al., 1982).

3. Methods

Methods include micro-CT analysis of molars, histological analyses of tusk and molars, isotope analyses of enamel by three methods, and application of forward and inverse models to molars (Table 1). Here we provide an abbreviated description of the methods; detailed methods are given in the Supplementary Information.

3.1. Micro-CT of molars

Two sectioned pieces of developing elephant molars (Table 1) were analyzed at the University of Utah's micro-CT facility. One is the fifth molar plate (from the mesial end) of Misha's lower right M3, hereafter Misha_Rm3.5. The molar plate was ~100 mm in length. The other is the ninth plate from a lower M1 (or M2) from K07-M53, hereafter K07-M53_m1.9, which was ~65 mm in length. For both specimens, a ~5 mm wide strip of enamel was cut from the distal side of the plate. CT scans were done using an Xradia Micro XCT-400 at 60 kV/10W at 4x magnification. Multiple scans, ~125 mm^3 in total volume, were done on each section with a resolution of 5.05 μm/voxel. Data were compressed to 8-bit grayscale stacks and analyzed in ImageJ (version 10.2) using linear, 10–25 pixel width grayscale profile scans normal to the EDJ. The densities of mature elephant molar enamel and tusk fragments were determined using a pycnometer and micro-CT scanned to develop a calibration curve to convert grayscale values to densities. Profiles were smoothed with a 10-point running mean and converted from grayscale to percent of maximum enamel density based on the density calibration.

3.2. Histological sample preparation and analysis

Thin sections of the distal side of molar plates were made from the same Misha_Rm3.5 section that was CT scanned, TE-95 m3 molar plate 7 (TE-95_Rm3.7), and an isolated enamel plate from the American Falls mammoth (IMNH-40368); (Table 1). Sections were cut and mounted on oversized slides, polished to 80–150 μm thickness using successively finer grits (down to 0.3 μm grit) on a lap. Photomicrographs, including the full enamel thickness and the EDJ, were taken of each specimen at 25-40x magnification and stitched into photomosaics (Figs. S2–S4). Additionally, enamel thickness was measured orthogonally from the EDJ to the outer enamel surface under the microscope. For the tusk dentin slab from Misha, M640, high resolution (9600 dpi) full color flat bed scans were made on cut and polished longitudinal and transverse surfaces (Supplementary Information; Figs. S5 and S6). Images were converted to grayscale images, contrast enhanced in Photoshop to highlight second-order (weekly) growth increments, and increment thicknesses were measured in ImageJ (Uno et al., 2020) using the plug-in IncMeas v1.2 (Rountrey, 2009). The longitudinal scan of M640 was used to measure the appositional angle, θ, of tusk dentin along the pulp cavity with respect to the tusk axis (Fig. S8). This angle is used to convert axial growth rate of the tusk measured by bomb ^{14}C methods (Uno et al., 2013) to radial growth rates, which can then be compared to histologically determined growth rates from the M640 transverse image (Fig. S7).

Crown formation times (CFTs) in the proboscidean teeth were measured following the methods of Dirks et al. (2012). Estimating CFT requires measurement of the angle of apposition, α, defined as the angle between the EDJ and the striae of Retzius (Figs. S2–4). A second measurement required is the daily secretion rate (DSR), defined as the

Table 1
List of analyses performed by sample ID and element on fossil and modern proboscidean molars and tusks. Conv. = conventional.

					Isotope profile			
Sample ID	Element	μCT	Thin section	Histological analyses	Conv.	Laser	μmill	^{14}C
Misha M640	tusk			X			X	X
R37-412	tusk		X	X			X	X
R37_Rm3.8	molar				X			X
Misha_Rm3.5	molar	X	X	X	X	X	X	
K07-M53_m1.9	molar	X						
TE-95_Rm3.7	molar		X	X				X
IMNH-40368	molar				X			
LACM-47129	molar				X			

thickness of enamel secreted per day along enamel prisms. This was done at 100x magnification. Using the DSR and α, the daily extension rate (DER) can be determined using trigonometric relationships. DER represents the daily length of crown extension from the tooth apex to the cervix, enabling determination of CFT. DSR, determined from daily growth increments, and the angle **α** were both measured from thin sections to calculate CFT.

3.3. Stable isotope sampling and analysis

One elephant tusk and four proboscidean molar plates were serially sampled to produce intratooth carbon and oxygen isotope profiles (Table 1). A slab of tusk dentin (Fig. S6) from Misha (M640) was micro drilled on the polished longitudinal surface using an end-milling technique (Supplementary Information *1.4.1*; Uno et al., 2020). Mill paths, 100–200 μm wide and 1 mm deep, were parallel to growth increments such that each sample represented *ca.* one to two weeks of time. Carbon and oxygen isotope data from an intratooth profile from another tusk dentin slab (R37-412) from elephant R37 are also used in the modeling in this study (Uno et al., 2020). The two tusk dentin profiles were selected because of their overlapping chronologies—based on bomb-curve ^{14}C determined growth rates—with corresponding molar plate intratooth profiles used in the study (Table 1). Details about their origin, number of samples, and ages are in the Supplementary Information. Drilled tusk dentin powder was pretreated with 30% H_2O_2 for 30 min, triple DI rinsed and dried (Supplementary Information).

Four molars were analyzed, two *L. africana* (Misha_Rm3.5 and R37_Rm3.8) and two *M. columbi* (LACM-47129 and IMNH-40368) (Table 1). Three sampling methods were used to generate stable carbon and oxygen intratooth enamel profiles: conventional drilling with a hand-held drill along the growth axis (Figs. S7 and S8); microdrilling (Merchantek micromill) using an end-milling technique, parallel to striae of Retzius along the growth axis from the outer enamel to the EDJ (Fig. S9); and laser ablation profiles from the EDJ to the outer enamel surface (Fig. S10). Conventionally and micro-drilled enamel samples were pretreated with H_2O_2 and buffered acetic acid as detailed in the Supplementary Information (Section 1.4.2). All samples were analyzed by dual inlet isotope ratio mass spectrometry as described in Supplementary Information Section 1.5. We calculate the half-life of body water in elephants using equations and methods detailed in Supplementary Information Section 1.6.

3.4. Forward and inverse models

Stable isotope data from conventionally drilled *L. africana* and M. columbi profiles are input into forward (Passey et al., 2002) and inverse (Passey et al., 2005) models. The model input parameters include f_i, l_a, and l_m, which are determined from micro-CT and histological analyses. The forward model is evaluated for *L. africana* by comparing the M640 intratooth tusk profile with the forward model results from the enamel profile of Misha_Rm3.5 (Fig. S7), both of which span the move from California to Utah in 2005. The inverse modeling was preformed using Matlab (version 7.10; R2010a), where 100 model solutions were performed to yield a mean estimated input (m_{est}), which represents the reconstructed diet (carbon) or body water (oxygen) input signal. Detailed model descriptions are in the Supplementary Information section 1.7.

4. Results

4.1. Micro-CT

Densities of tusk dentin and fully mature molar enamel measured by gas-displacement pycnometry yield values of 1.84 and 3.34 g/cm3, respectively, with uncertainties of *ca.* ± 5%. The tusk dentin value is lower than that of ~2.2 g/cm3 observed by Weatherell et al. (1974) in human teeth. The elephant enamel value is slightly higher but within ~15% of the density reported for human enamel (Weatherell et al., 1974), and it is close to the value for pure apatite (3.15–3.2 g/cm3). From this point forward, density results are presented as a percent of final enamel density (%FD).

A total of 22 density profiles normal to the EDJ were measured in the two molar segments (Fig. 3). Profiles were taken along Misha_Rm3.5 from 94.6 to 3.5 mm above the base of the plate (Fig. 3A) and along K07-M53 from 38 to ~1 mm from the base (Fig. 3B). In general, the density profiles from ~40 to 0 mm are very similar in both molar plates. For example, the two profiles near the base of Misha_Rm3.5 (7.5 and 3.5 mm), have mean densities of 79.6 and 79.9 %FD, respectively, similar to 77 %FD at 3.8 mm in K07-M53.

All density profiles ~35 mm above the cervix or higher show a sharp decrease from nearly 100 %FD at the EDJ to *ca.* 60 %FD at the outer enamel surface (Fig. 3). The break in slope in the density profile moving from the EDJ toward the outer enamel surface marks the location of the maturation front in each profile. Maturation length, l_m, is determined by plotting the distance from the EDJ where the break in slope occurs versus the position of the profile above the cervix (Fig. 4). This defines the maturation front. Dividing the enamel thickness by the slope of this line yields l_m, which is 69.8 ± 4.8 mm, where the uncertainty is calculated from the slope error. The maturation angle is 2.49 ± 0.17°.

The immature enamel from profiles from the lower part of the molar plates is used to determine the initial enamel density, f_i. Four density profiles from within 1.25 to 0.1 mm of the base of K07-M93 yield a mean f_i of 64.5 ± 1.8 %FD (±1σ) (Fig. 3B). The f_i of enamel from within the interval of 150 to 100 μm from EDJ from the same four profiles is essentially the same (63.6 ± 1.7 %FD). However, moving several millimeters up along the plate, enamel at the EDJ increases to 70 and 77 % FD at 3.75 and 2.5 mm above the cervix. In nearly all profiles where enamel thickness exceeds 1 mm (Fig. 3A), the outermost enamel has a density of 55–65 %FD, suggesting that outer enamel f_i is equal to or slightly less than the f_i near the EDJ, which is ~65 %FD.

4.2. Histological analyses

4.2.1. Tusk thin sections

The thicknesses of 246 consecutive second-order growth increments are plotted for Misha tusk dentin slab 640 in Fig. 5A and the data are in Table S1. Mean thickness is 139 ± 38 μm (Table 2; uncertainty is reported as 1σ here and elsewhere, unless specified). The range is 67–240 μm. If weekly (i.e., exactly 7 days) periodicity is assumed, then the mean daily (radial) growth rate is 19.9 ± 5.4 μm/day (Table 2) with a range of 9.6–34.2 μm/day, and the total time in slab M640 is 1722 days (4.71 years) (Fig. 5B). Although the daily growth rate varies from ~10 to 34 μm/day, it appears generally linear over the 4.7 years represented in slab M640 (Fig. 5B).

An independent calculation of the radial growth rate from the M460 tusk dentin slab can come from measurements of the angle θ between the tusk axis and growth increments (Fig. S8; Table S2). This yields a mean θ value of 7.7 ± 0.4° (n = 7) (Table S1). The overall axial growth rate of Misha's tusk determined by bomb-curve ^{14}C age dating, 51.1 ± 7.4 mm/year (Uno et al., 2013) can be converted to a radial growth rate using the tangent of θ (Table S2). This produces a radial growth rate of 19.0 ± 3.0 μm/day, which is within 5% of the value determined by histological methods (Table 2). Both calculated radial growth rates for M640, 19.9 ± 5.4 μm/day by second order growth increments and 19.0 ± 3.0 μm/day by ^{14}C, are similar to a mean radial growth rate of 18 ± 8.2 μm/day determined from counting third-order (daily) increments (n = 336) in Misha thin section M720 (Uno, 2012).

A final approach for determining the radial growth rate comes from using the stable isotope data as a time marker for the date of Misha's move to Utah on April 22, 2005, which is presented in section 4.2.1. The date of death (Sept. 9, 2008) is represented by the pulp cavity surface. The distance between the two points on slab M640 (18.14 mm) divided

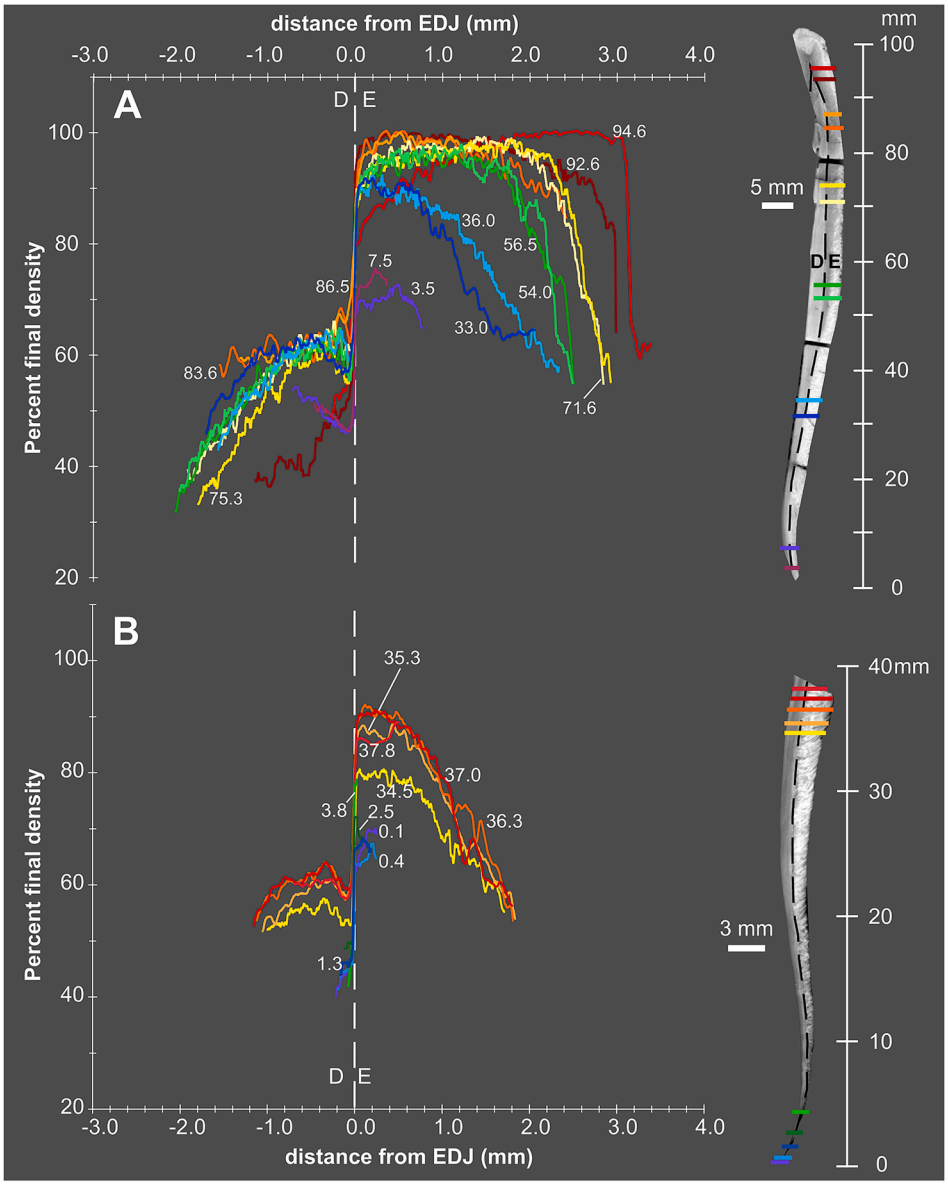

Fig. 3. Micro-CT transects normal to the EDJ in two molar sections from A) Misha_Rm3.5 and B) K07-M53_m1.9. Grayscale images of specimens are shown at right, each with different length and width scales. Colored lines correspond to distance (mm) from the base of the plate. Dentin (D) is to the left and enamel (E) to the right in the plots and images.

by the total time she lived in Utah (1236 days) yields a growth rate of 14.7 ± 0.8 μm/day, which is ~25% less than the 14C and histological results (Table 2). Tusk growth rates are variable and it is possible that Misha's tusk growth rate slowed after the move.

4.2.2. Molar thin sections

The appositional angle, α, was measured along the three molar thin sections wherever feasible (Table S3). Misha's fifth molar plate was still developing at death and had a relatively high organic content in the immature enamel in the lower half of the plate. The organic matter interfered with the optics of transmitted light microscopy so that much of the immature or partially mature enamel appears opaque or blurred in thin section. Mature enamel on the other hand, has clearly discernible histological features that include enamel prisms, daily growth increments, and striae of Retzius (Figs. S3, S4, and S5). Four measurements of α were made along Misha_Rm3.5, and have a mean value of 3.3 ± 0.5° (Fig. 6A). The measurements from the TE-95 thin section (n = 16; Table S3) yield a mean value of 3.4 ± 0.4° with a range of 2.8–4.8° (Fig. 6B). In both molars, there is an increase in α toward the cervix that is best described by a logarithmic curve (Fig. 6). A single logarithmic regression for all elephant data (Misha and TE-95) may be appropriate as well. The combined mean angle of apposition from both elephants (α_{LFN}), except in the lower 25 mm where α increases rapidly, is 3.2 ± 0.2°. A linear regression of α_{LFN} from the occlusal surface to 25 mm above the cervix yields a shallow slope of −0.003°/mm (R^2 = 0.18), indicating that α_{LFN} is essentially constant from the apex of the plate down to about 25 mm above the cervix. Enamel thickness was also measured on the two elephant thin sections and the thick section of R37_Rm3.8. Thickness was measured normal to the EDJ out to the enamel edge (Table S4). Enamel thickness is greatest at the distal tip of the molar plate and thins to ~0.5 mm or less at the cervix. For the two plates where measurements were made on the distal portion of the plate, thicknesses ranged from ~3.5 to 2.5 mm until 30 mm from the base of the plate, where enamel thickness decreases rapidly (Fig. S11).

The appositional angle in the mammoth molar ($\alpha_{mammoth}$) is greater than in elephants, and there is a relatively greater increase in $\alpha_{mammoth}$ at

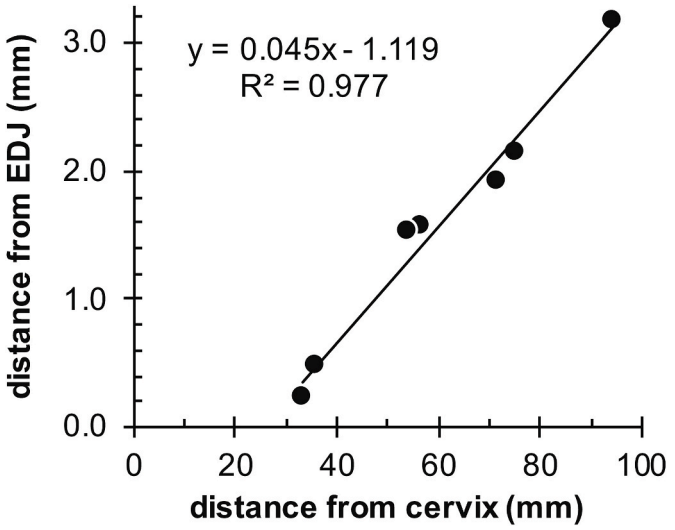

Fig. 4. The break in slope in a density profile normal to the EDJ indicates the position of the maturation front. Plotted here is the location of the break in slope (mm from the EDJ) vs. the position of the density profile above the cervix (mm). The maturation length (l_m) is 69.8 ± 4.8 mm.

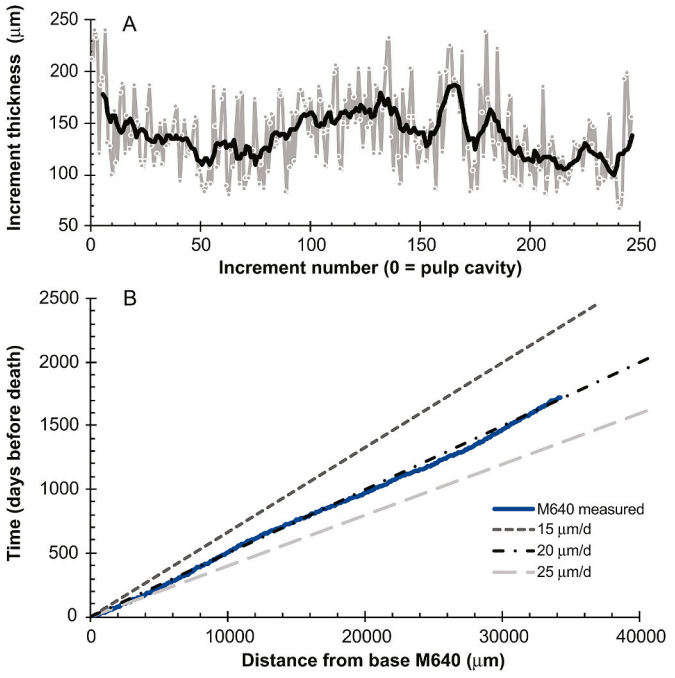

Fig. 5. Histological data from tusk dentin slab M640. A) Second-order increment thickness vs. increment number with raw data in grey and a 10-point running average in black. B) Sum of increments from the base of M640 vs. number of days before death, assuming each second-order increment represents seven days. Given this assumption, the growth rate (blue line) is approximately constant (20 µm/day). Modeled growth rates of 15, 20, and 25 µm/day are shown for comparison. (For interpretation of the references to color in this figure legend, the reader is referred to the Web version of this article.)

the base of the plate than observed in elephants (Fig. 6B). The mean $\alpha_{mammoth}$ value is 6.9 ± 2.0° (n = 24) with a range of 11.8 to 4.2° (Table S3). If the high angles observed in the lower 25 mm of the plate are excluded, then the mean $\alpha_{mammoth}$ decreases to 5.8 ± 0.7°. As with the elephant molars, the angle of apposition is best described by a logarithmic function.

Appositional length, l_a, can be calculated from enamel thickness and

Table 2
Summary of growth rates in tusks and molars by different methods. M640, Misha_Rm3.5 and TE-95_Rm3.7 are *Loxodonta africana* and IMNH-40368 is *Mammuthus columbi*. Input values for calculations are in Supplementary Tables.

Dental element	Sample ID	Growth Rate (µm/day)	1σ (µm)	Growth Rate (mm/y)	1σ (mm)	Method
Tusk	M640 radial	19.9	5.4	7.3	2.0	increment thickness
Tusk	M640 radial	19.0	3.0	6.9	1.1	angle θ & ^{14}C
Tusk	M640 radial	14.7	2.3	5.4	0.9	angle θ & isotopes
Tusk	M640 axial	143.4	10.5	51.1	3.8	angle θ & ^{14}C
Molar	Misha_Rm3.5	55.3	8.6	20.2	3.1	angle α & DSR
Molar	TE-95 Rm3.7	52.6	7.5	19.2	2.7	angle α & DSR
Molar	TE-95 Rm3.7	44.6 [a]	0.2	16.3	0.1	^{14}C
Molar	IMNH-40368	35.0	6.3	12.8	2.3	angle α & DSR

[a] Previously published in Uno et al. (2013) and included here for comparison with histological methods.

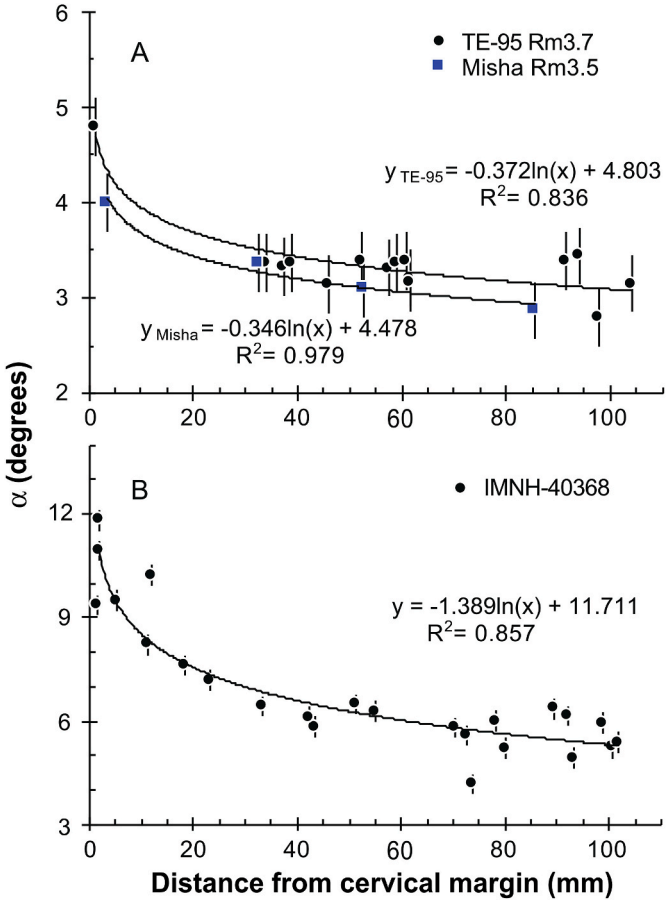

Fig. 6. Plots of α vs. distance from the cervical margin for two proboscidean species, A) *Loxodonta africana* and B) *Mammuthus columbi*, where α is the angle of apposition measured between the striae of Retzius and the EDJ.

α, where l_a = enamel thickness/tan α. Using this approach on the two elephant molar thin sections and limiting the region of interest to 25 mm or higher above the cervix, the mean l_a for elephant molar plates is 55.6 ± 4.3 mm (n = 14). Due to the rapid decrease of enamel thickness and

the steepening of α near the cervix, l_a diminishes to 14 mm and 9 mm at 3.6 and 1.3 mm above the cervix. The l_a calculated with this method from mammoth molar IMNH-40368 is 29.4 ± 3.5 mm using an enamel thickness of 3 mm and an α of 5.8 ± 0.7°.

An alternative method for determining l_a is through measurement on the surface of developing molar plates. The appositional surface is smooth and chalky, whereas enamel in the maturation phase is rugose. Measurements of l_a from plates of developing molars K07-M53 and TE-95 ranged from 31.8 to 48.9 mm. Both molars had a diminutive posterior plate that indicated molar formation was nearing completion. Thus, l_a values determined by this method may represent minimum values as the plates may have completed (or nearly completed) crown extension.

A third method for measuring l_a is to trace prominent striae of Retzius from the EDJ to the outer enamel surface. The distance measured along the outer enamel surface between those two points gives the l_a. This was done on the Misha and TE-95 thin sections and yielded a mean l_a value of 45.5 ± 2.0 mm (n = 4) with a range of 43.5–48.3 mm. In several cases, the outermost 200 to 500 μm of enamel had spalled off, probably while preparing the thin section, and thus, the intersection with the outer enamel surface had to be estimated.

CFT was calculated from α and DSR values. The DSR was measured in thin section TE-95 (at 100x) in a single transect at ~80 mm above the cervix. Mean DSR is 3.0 ± 0.4 μm (n = 24) with a range of 2.20–3.83 μm. The α value is calculated as a function of distance from the cervix using the logarithmic regression equations in Fig. 6. Although DSR likely varies throughout formation of a plate, a value of 3 μm is used as a basis for calculating CFT in the two elephant molars, and a DSR of 3.5 ± 0.5 μm is used to calculate CFT of the mammoth molar based on data from Dirks et al. (2012). CFT represents the time required for molar plate to grow to its full length, but this is less than the total formation time of a molar plate because it does not account for enamel maturation that continues after the secretory phase is completed. CFTs are modeled using constant DSRs of 2, 3, and 4 μm/day for the two elephant molars (Fig. 7A–B) and DSRs of 3, 3.5, and 4 μm/day for the mammoth molar (Fig. 7C).

The mammoth plate is worn to a height of ~103 mm. An initial crown height of 180 mm is assumed based on published data for a mammoth molar plate (Dirks et al., 2012), although this is an approximation. CFT for the three molars range from 3.6 to 9.0 years for the elephant molar plates and 9.7–12.9 years for the mammoth plate (Table 3). A linear growth rate appears to be appropriate for profiles in elephant molar plates, which have calculated growth rates of 20.2 ± 3.2 mm/yr for Misha Rm3.5 and 19.2 ± 2.8 mm/yr for TE-95 Rm3.7, assuming a DSR of 3 μm/day based on measurements in TE-95 (Table 2, Fig. 7A). The mammoth plate from IMNH-40368 has a calculated growth rate of 12.8 ± 2.3 mm/yr (Table 2). An l_m of 70 ± 5 mm, based on the micro-CT data, and a growth rate of *ca.* 20 mm/year yield a relatively long enamel maturation time of 3.2 ± 0.2 years.

4.3. Carbon and oxygen isotope profiles in tusks and molars

4.3.1. Micromill isotope data from tusks

The full profiles of $\delta^{13}C$ and $\delta^{18}O$ values from Misha tusk dentin slab M640 are plotted in Fig. S12 (n = 97) and the data are available in Table S5. For comparison to the coeval enamel isotope profiles from Misha_Rm3.5, we show the latter part of the record (Fig. 8A). The mean $\delta^{18}O$ values during the CA and UT portions of the tusk dentin are −9.3 ± 0.8‰ and −12.9 ± 0.8‰, respectively. However, taking $\delta^{18}O$ values just before and after the move yields a shift of *ca.* −5‰ between CA and UT (Fig. 8A). We calculate a half life ($t_{1/2}$) of body water of 7.8 ± 2.6 (1σ) days.

The $\delta^{13}C$ data indicate that Misha had a C_3-dominated diet in UT during the time interval represented in M640, but had a highly variable diet during the last 2 years in CA (Fig. S12, Fig. 8). Mean $\delta^{13}C$ values for CA and UT are −7.7 ± 2.5 and −13.3 ± 0.6‰. The $\delta^{13}C$ values from just before and after the move from CA to UT differ by −8.3‰. The magnitude of the $\delta^{13}C$ and $\delta^{18}O$ shifts in the tusk dentin profile are used as a baseline for comparison with molar profiles from laser, micromill, and conventional sampling methods.

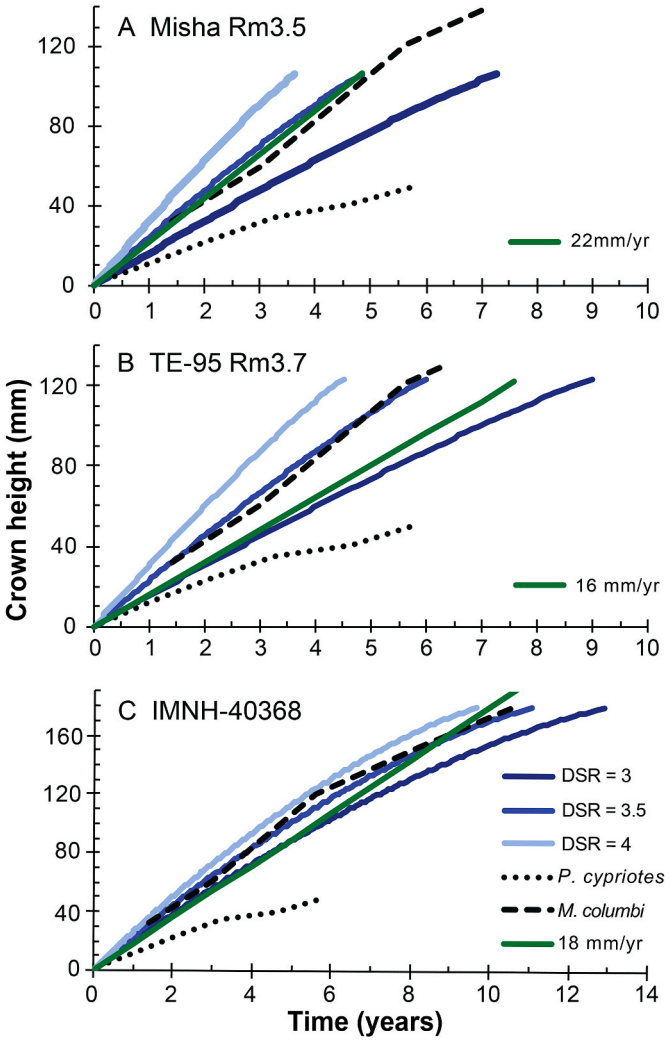

Fig. 7. Modeled crown formation time (years) for two *L. africana* molar plates (A and B) and *M. columbi* (C) using constant daily secretion rates (DSRs). Appositional angles (α) are from the logarithmic regressions in Fig. 6. Data from *Palaeoloxodon cypriotes* and *M. columbi* (in black) are from Dirks et al. (2012). Green lines represent modeled constant growth rates; for TE-95, the ^{14}C-based growth rate of 16 mm/year is modeled. (For interpretation of the references to color in this figure legend, the reader is referred to the Web version of this article.)

Table 3
Modeled crown formation time (CFT) in years for three proboscidean molar plates. Misha_Rm3.5 and TE-95_Rm3.7 are *Loxodonta africana* and IMNH-40368 is *Mammuthus columbi*. Modeled results assume constant daily secretion rates (DSR). DSR values in microns per day.

Thin section	CFT (years)		
	DSR = 2	DSR = 3	DSR = 4
Misha_Rm3.5	7.26	4.84	3.63
TE-95_Rm3.7	9.00	6.00	4.50
	DSR = 3	**DSR = 3.5**	**DSR = 4**
IMNH-40368	12.89	11.05	9.67

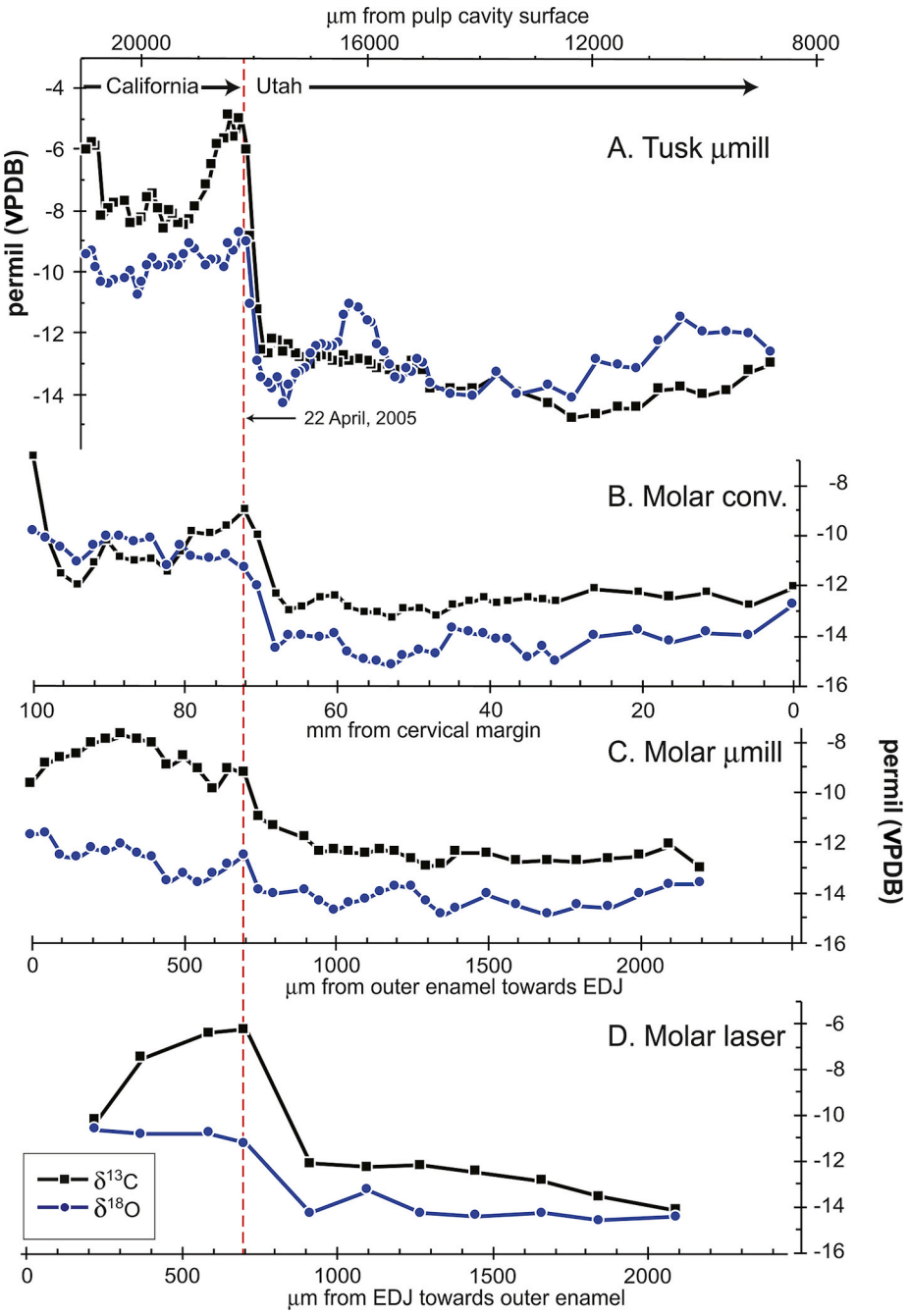

Fig. 8. Intratooth $\delta^{13}C$ and $\delta^{18}O$ profile values from A) Misha tusk dentin slab M640 and from molar enamel of Misha_Rm3.8 sampled by three methods. B) A conventionally drilled profile from the occlusal surface to the cervical margin, C) a micromilled profile at a resolution of 50 µm per sample drilled parallel to the appositional surface, and D) a LA-GC-IRMS profile (250 µm spot size) from the EDJ to the outer enamel surface (Fig. S14). The move from CA to UT occurs in late April 2005 (red dashed line) and results in a sharp decrease in both $\delta^{13}C$ and $\delta^{18}O$ values. (For interpretation of the references to color in this figure legend, the reader is referred to the Web version of this article.)

4.3.2. Conventional isotope data from enamel

The $\delta^{13}C$ and $\delta^{18}O$ values (n = 42) from conventional drilling of Misha_Rm3.5 are plotted in Fig. 8B and data are available in Table S6. Overall, the conventionally drilled profiles have similar structure to the M640 tusk dentin profile, and the enamel and tusk dentin profile overlap from early 2004 through January 2007 (Fig. 8). The isotopic shift associated with the move occurs 72.2 mm above the cervix (Fig. 8B). The shifts in $\delta^{13}C$ and $\delta^{18}O$ are −4.0‰ and −3.4‰, respectively. Similar features in the $\delta^{18}O$ profiles include two periods where $\delta^{18}O$ values increase 2–3‰ while Misha was in UT (Fig. 8).

There is an offset between enamel and tusk isotope data (δ_{enamel} - δ_{tusk}) that formed after the move to UT (Table 4). This long-term offset observed over a period of ~1.5 years may be a result of differences in pretreatment of tusk dentin and enamel or due to slight differences in fractionation factors or mineralization processes in dentin versus enamel. A correction factor of +0.7‰ for $\delta^{13}C$ and −1.3‰ $\delta^{18}O$ is

Table 4
Mean $\delta^{13}C$ and $\delta^{18}O$ values for all Misha enamel and tusk apatite that formed during her time in Utah (2005–2009). All enamel values are in agreement, whereas tusk dentin is ~0.6‰ depleted in ^{13}C and enriched ~1.4‰ in ^{18}O compared to conventional enamel. Laser values are corrected to conventional (acid digestion) values using $\varepsilon^*_{laser\text{-}acid}$ values of −0.7‰ for carbon and −7.4‰ for oxygen (Supplementary Information).

		‰				
Sample ID	Sampling method	$\delta^{13}C$	1σ	$\delta^{18}O$	1σ	n
Enamel						
Misha _Rm3.5	conventional	−12.7	0.3	−14.3	0.5	26
Misha _Rm3.5	micromill	−12.4	0.3	−14.2	0.4	17
Misha _Rm3.5	laser	−12.6	0.5	−14.2	0.6	7
Tusk Dentin						
Misha_M640	micromill	−13.3	0.6	−12.9	0.8	45

applied to the tusk profile used in the models so that isotope ratios from the tusk and tooth are in agreement based on the long-term Utah values.

The $\delta^{13}C$ and $\delta^{18}O$ values (n = 39) from conventional drilling of R37_Rm3.8, the Samburu NR elephant, are listed in Table S6. The mean $\delta^{13}C$ value is −10.8 ± 0.3‰ with a range of 1.2‰, and mean $\delta^{18}O$ is −1.3 ± 0.3‰ with a range of 1.3‰. As with the Misha tusk and enamel data, there is an offset between the two profiles, and corrections were applied so that the isotope values in both profiles were in agreement.

Fossil mammoth enamel values from LACM-47129 (n = 22) and IMNH-40368 (n = 46) are also listed in Table S6. The mean $\delta^{13}C$ value of the Rancho La Brea mammoth (LACM-47129) is −6.7 ± 1.4‰ with a range of 3.7‰, indicating a variable mixed C_3-C_4 diet. The mean $\delta^{18}O$ is −1.7 ± 0.4‰ with a range of 1.5‰. The mean $\delta^{13}C$ value of the Idaho mammoth (IMNH-40368) is −9.8 ± 0.5‰ with a range of 2.0‰, indicating a fairly constant C_3 diet. The mean $\delta^{18}O$ is −13.3 ± 0.3‰ with a range of 1.8‰.

4.3.3. Micromill isotope data from enamel

The $\delta^{13}C$ and $\delta^{18}O$ values (n = 36) of enamel micromilled from Misha_Rm3.5 are plotted in Fig. 8C and data are listed in Table S7. The mean $\delta^{13}C$ value is −10.8 ± 1.9‰ with a range of 5.3‰, and mean $\delta^{18}O$ is −13.5 ± 0.9‰ with a range of 3.2‰. Data from micromilled portions of the molar that formed in Utah are compared to laser and conventional data, as well as the tusk dentin isotope data, to further evaluate the isotopic offsets between sampling type and tissue type (Table 4). The isotopic shift is −3.1‰ and −2.2‰ for $\delta^{13}C$ and $\delta^{18}O$, respectively. Sample yield, measured as millivolts per microgram (mV/μg) of sample digested, is plotted as a function of distance from the EDJ (Fig. S13). The linear decrease in yield from the EDJ toward the outer enamel surface suggests a linear maturation geometry. This linear decrease in yield could also result from other maturation geometries, but this alternative is less likely.

4.3.4. Laser ablation isotope data from enamel

The $\delta^{13}C$ and $\delta^{18}O$ values from the three laser profiles are plotted in Fig. S14 and listed in Table S8. Laser values are corrected to conventional (acid digestion) values using $\varepsilon^*_{\text{laser-acid}}$ values of −0.7‰ for carbon and −7.4‰ for oxygen. These are based on paired laser-acid analyses and background is given in Passey and Cerling (2006). Scans that produced charred ablation pits indicate the presence of organic matter and resulted in anomalous isotope values. These data are not plotted or considered in evaluation of profile data, but are included in Table S8. A temporal shift between profiles, which were placed 10–15 mm apart along the growth axis of the tooth (Fig. S10), is evident in the isotope data (Fig. S14). The enamel at 80 mm above the cervix formed earliest, and the isotopic shift associated with the move is not present in that scan (Fig. 13A), although scans removed due to charred pits suggest the shift may occur near the outer enamel surface (~2600 μm). The diet shift from C_4 to C_3 and back to C_4 that occurred in mid–2004 (Fig. S12) is however, recorded in the 80 mm profile.

The profile from 71 mm above the cervix records the isotopic shift associated with the move at 1700 μm above the EDJ (Fig. S14B). The shifts in $\delta^{13}C$ and $\delta^{18}O$ are −6.1‰ and −3.3‰, respectively. The profile from 54 mm has the simplest structure of the three profiles with the shift associated with the move at 700 μm from the EDJ (Fig. 13C). The shifts in $\delta^{13}C$ and $\delta^{18}O$ are −5.9‰ and −3.1‰, respectively, which are nearly identical to those from the 71 mm profile.

The CO_2 yields for each laser scan are plotted as a function of distance from the EDJ (Fig. S15). Yield is a function of the carbonate mineral content, and thus serves as a proxy for apatite mineral density per unit volume ablated. The decrease in yield from the EDJ toward the outer enamel surface also suggests a linear maturation phase, which is in agreement with the micromill yield data (Fig. S13).

4.4. Modeling results

4.4.1. Forward model

The micro-CT, histological, and stable isotope results from the molars and tusks provide data necessary to test whether the forward model of Passey and Cerling (2002) is applicable to elephant molar plates. Forward model parameters are $f_i = 0.65$, l_a = (35, 45, and 55 mm), and $l_m = 70$ mm. Isotope data from enamel profiles values are smoothed with a three-point weighted mean (0.25, 0.5, 0.25) for all modeling work. Since each method for measuring l_a yielded different results (37 mm by visual methods, 45 mm by tracing striae of Retzius, and 56 mm by thin section trigonometric calculations), forward model results using 3 different l_a values (35, 45 and 55 mm) are shown for Misha_Rm3.5 (Fig. 9). Forward model results using tusk intratooth profile data (Fig. 8A) as the primary input signal are generally in good agreement with measured enamel values (Fig. 9). For carbon, there is a temporal offset in the beginning of the record and the modeled enamel curves lag the measured data across the move by up to four months. Another region of misfit is just before the move, where modeled $\delta^{13}C$ values are up to 1‰ greater than measured enamel values. For oxygen, modeled curves are close to the measured enamel curve in overall structure, but under-predict the $\delta^{18}O$ value by ~1‰ prior to the move. A temporal offset is present and most pronounced at the beginning and end of the modeled interval.

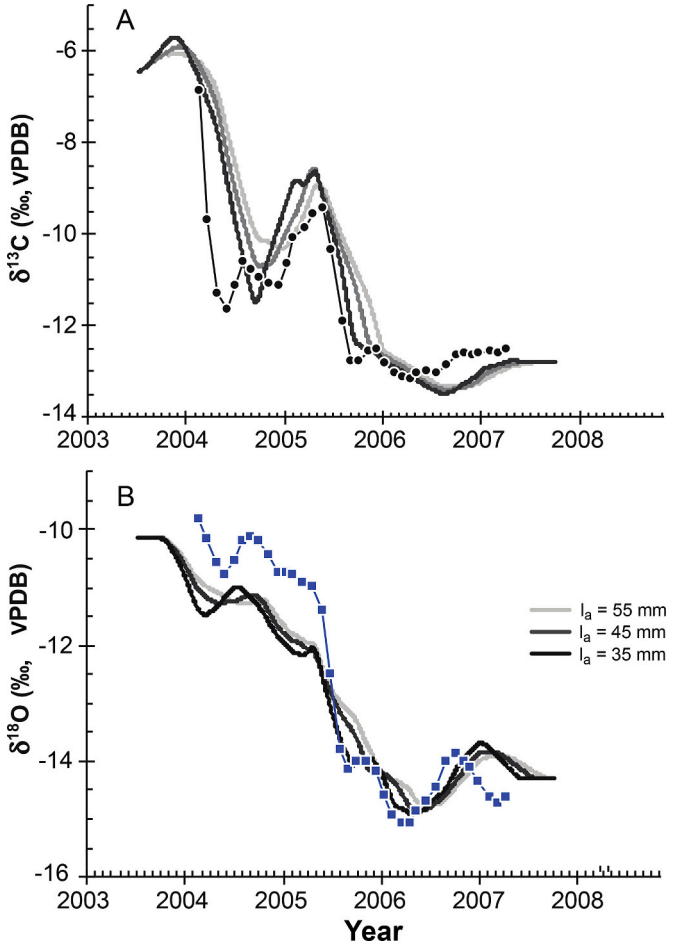

Fig. 9. Forward model results for A) $\delta^{13}C$ and B) $\delta^{18}O$ from conventional sampling of molar Misha_Rm3.5. The three grey lines represent l_a values of 35, 45, and 55 mm. Measured enamel data have been smoothed with a 3-point weighted average and are shown in A) as black circles and in B) as blue squares. (For interpretation of the references to color in this figure legend, the reader is referred to the Web version of this article.)

Model results from R37 are presented in Fig. 10. The primary input signal for the model is isotope profile data from tusk dentin slab R37-DEN-412 (Uno et al., 2020). An l_a of 35 mm was selected for plate R37_Rm3.8 for two reasons. First, plate height (76 mm) is approximately 75% of the height of the Misha and TE-95 plates from which the longer l_a values were derived, and it follows that l_a might scale with final plate height. Second, using an l_a of 45 mm or greater removed nearly all amplitude from the modeled isotope profiles. The approximate period over which molar plate R37_Rm3.8 formed is estimated as 1981 to 1987 based on ^{14}C data from the adjacent molar plate, R37_Rm3.7 (Uno et al., 2013). Visual matching of $\delta^{13}C$ profiles was used to align the forward model results to the measured enamel data (Fig. 10A). The modeled and measured data overlap for a period of *ca.* 3 years, and there is good agreement between the two. Agreement with the measured data is fairly poor, however, for most of the $\delta^{18}O$ forward model output (Fig. 10B), and this suggests the two profiles are not synchronized correctly. Measured $\delta^{18}O$ data show a peak with amplitude of ~0.7‰ that occurs in late 1985, which is not present in the model results.

In evaluating forward model results, it is important to keep in mind that temporal offset between model and measured data can have two sources: error in growth rates from the tusk or from the molar. The differences observed between the modeled and measured isotope values can be a result of incorrect model parameters or they can arise from incorrect assumptions about the tusk profile being representative of the primary input signal. This will be addressed in greater detail in the discussion below.

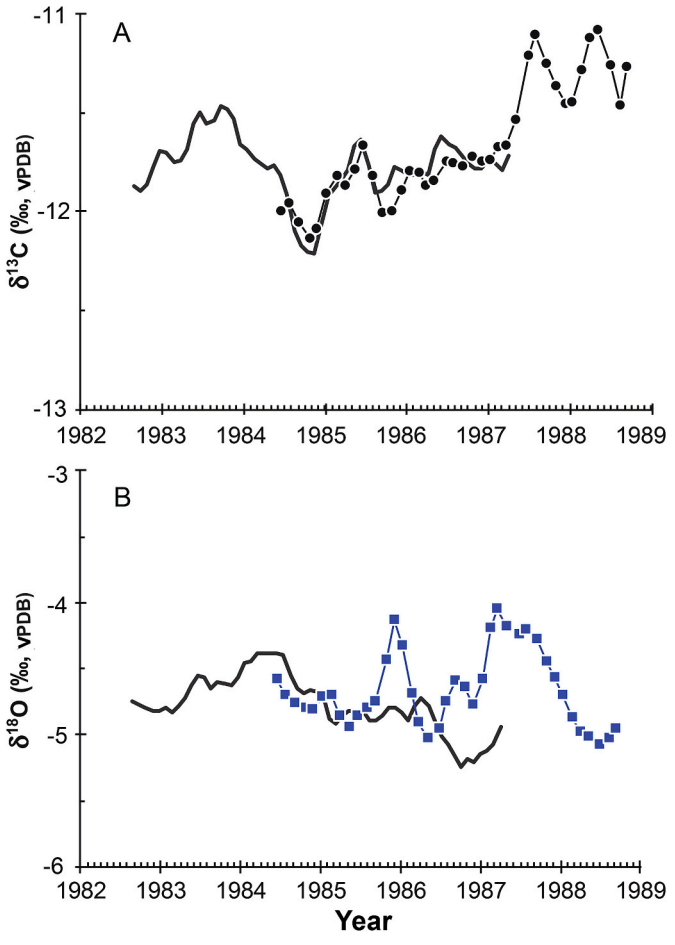

Fig. 10. Forward model results (l_a = 35 mm) for A) $\delta^{13}C$ and B) $\delta^{18}O$ from conventional sampling of molar R37_Rm3.8. Measured enamel data have been smoothed with a 3-point weighted average and are shown in A) as black circles and in B) as blue squares. (For interpretation of the references to color in this figure legend, the reader is referred to the Web version of this article.)

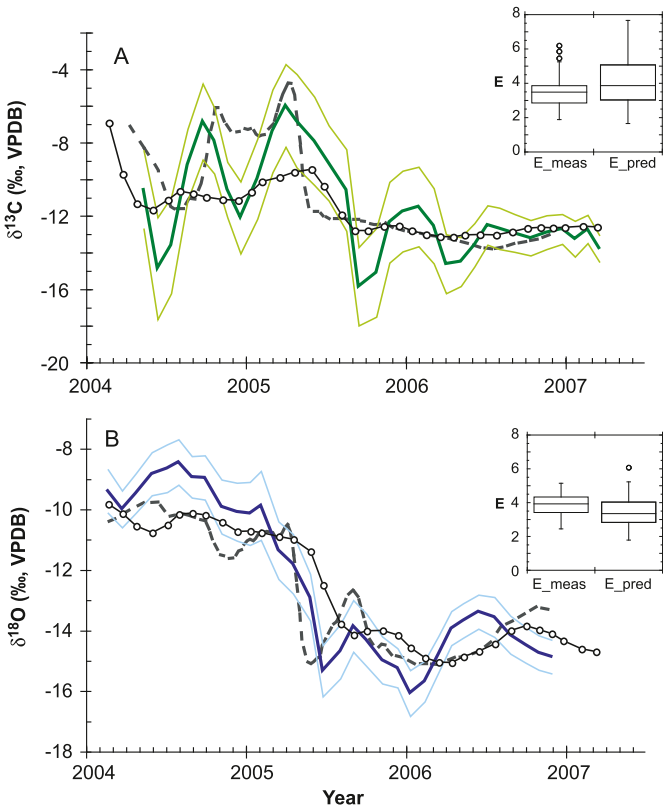

Fig. 11. Inverse model results for A) $\delta^{13}C$ and B) $\delta^{18}O$ from conventional sampling of molar Misha_Rm3.5. Bold colored line is the mean m_{est} from 100 solutions (±1σ). The dashed grey line is the primary input from tusk dentin profile M640, and circles are measured data from the molar Misha_Rm3.5. In both models l_a = 45 mm, l_m = 70 mm, openindx = 0.65*l_a, r2($\sigma_{\Delta x}$) = 0.2 mm, and r3($\sigma_{\Delta z}$) = 0.3 mm. A) r1(σ_{ms}) = 0.12‰,ε^2 = 0.005, and a reference vector (RV, see Supplementary Information) of −6 to −10‰; B) r1(σ_{ms}) = 0.22‰, ε^2 = 0.024, and RV of −11 to −14‰.

4.4.2. *Inverse model*

Inverse model results (m_{est}) from two elephant and two fossil mammoth molar profiles are given as the mean of 100 solutions (±1σ). Results from elephant molars are presented first because they include a known primary input signal from the tusk profile data and thus offer a way in which the inversion results can be directly evaluated. All plots showing inversion results (m_{est}) and measured enamel profiles also include boxplots comparing measured error (E_{meas}) and prediction error (E_{pred}) (see Passey et al., 2005 for equations).

Misha_Rm3.5 profile results are shown in Fig. 11. The primary input signal is the M640 isotope profile smoothed with a five-point median. A median filter was selected because it preserves edges better than a moving average filter. The estimated $\delta^{13}C$ profile, m_{est_C}, is shifted +80 days for comparison to the primary input signal. The profile nearly reaches the −4 to −5 $\delta^{13}C$ values associated with the 2004–2005 diet change in CA, but over-predicts the $\delta^{13}C$ values when diet changes from C_4- to C_3-dominated. The rapid shift in the primary input signal associated with the move occurs over a longer period (5 months) in m_{est_C} than in the tusk profile (~3–4 weeks). There is oscillation in m_{est_C} after the isotope shift associated with the move that first under-predicts and then over-predicts the $\delta^{13}C$ value of enamel. The $\delta^{13}C$ value of Misha's diet was relatively constant in UT, and m_{est_C} matches this value in the latter part of the enamel and primary input signals.

The estimated $\delta^{18}O$ profile (m_{est_O}) does a better job than m_{est_C} at recovering the primary input signal (Fig. 11B). M_{est_O} recovers the main features of the primary input signal, which include the shift associated with the move and periods of variability in the primary input signal that

occurred before and after the move. In particular, m_{est_O} shows the period of increased $\delta^{18}O$ values just after the move to UT, around late summer of 2005. There are minor offsets ($\leq$1‰) between the measured (primary input signal) and modeled (m_{est_O}) $\delta^{18}O$ values and in the temporal scale.

Inverse model results from the R37_Rm3.8 profile are plotted in Fig. 12. The five-point median smoothed R37-DEN-412 profile serves as the primary input signal. No temporal shift of m_{est_C} is required for comparison to the primary input signal. M_{est_C} tracks the periodicity and amplitude of the primary input signal quite well for the first two years of the record, but the two signals differ in the latter portion of the record. M_{est_O} and primary $\delta^{18}O$ input signals show little agreement. This is to be expected considering the similar poor fit observed in the forward model. Results from the R37_Rm3.8 should be interpreted with caution as there remains uncertainty as to whether or not visual matching of the tusk and molar profiles is correct.

Model parameters for mammoth molar profiles are based on histological results (l_a = 30 mm) and micro-CT results from elephant molars (f_i = 0.65 and l_m = 70 mm). The mammoth molars were sampled opportunistically (e.g., they were found in the lab) without any prior knowledge of the specimens, and in this regard, the results are fortuitous because the resulting profiles are quite different. The enamel profiles from LACM-47129 (Fig. 13), particularly for $\delta^{13}C$, have a periodic structure, whereas the profiles from IMNH-40368 are nearly constant throughout their entirety with the exception of several samples near the cervix (Fig. 14). Although the true primary input signals are unknown, the contrasting profiles offer an opportunity to test the inverse model on profiles that suggest two very different dietary and, to a lesser degree,

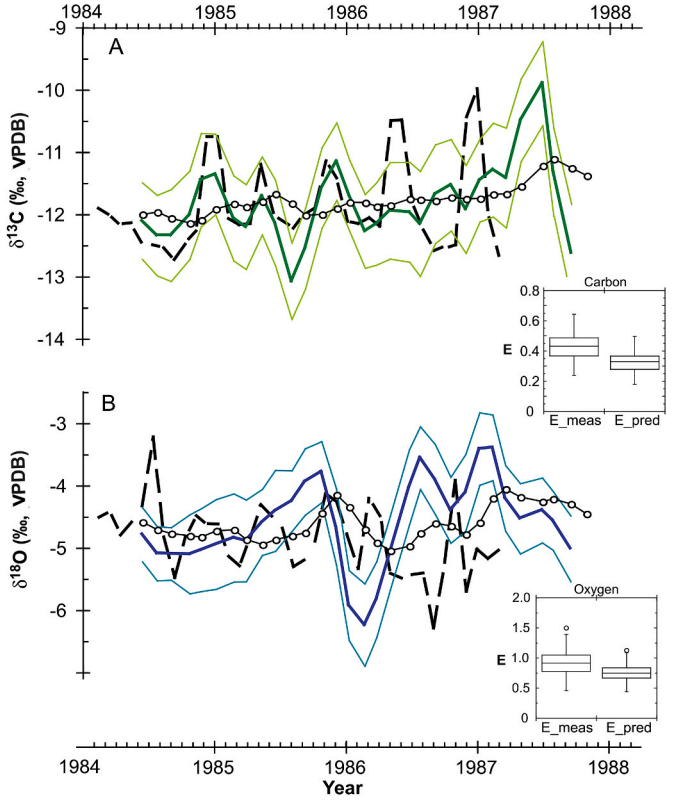

Fig. 12. Inverse model results for A) $\delta^{13}C$ and B) $\delta^{18}O$ from conventional sampling of molar R37_Rm3.8. Bold colored line is the mean m_{est} from 100 solutions ($\pm1\sigma$). The dashed grey line is the primary input from tusk dentin profile R37-412, and circles are measured data from the molar R37_Rm3.8. In both models l_a = 45 mm, l_m = 70 mm, openindx = 1, r2($\sigma_{\Delta x}$) = 0.2 mm, and r3 ($\sigma_{\Delta z}$) = 0.3 mm. For A) r1(σ_{ms}) = 0.1‰, ε^2 = 0.0035, and the reference vector (RV) is −11 to −12‰ and for B) r1(σ_{ms}) = 0.15‰, ε^2 = 0.012, and RV is −3 to −6‰.

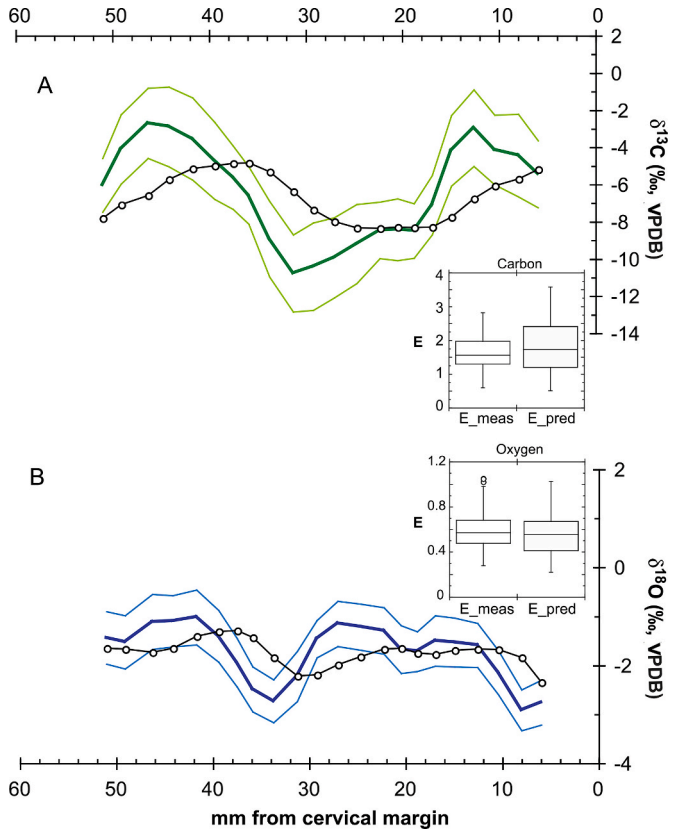

Fig. 13. Inverse model results for A) $\delta^{13}C$ and B) $\delta^{18}O$ from conventional sampling of mammoth molar LACM-47129. Bold colored line is the mean m_{est} from 100 solutions ($\pm1\sigma$) and circles are measured data. In both models l_a = 30 mm, l_m = 60 mm, openindx = 0.75*la, r2($\sigma_{\Delta x}$) = 0.5 mm, and r3($\sigma_{\Delta z}$) = 0.5 mm. For A) r1(σ_{ms}) = 0.1‰, ε^2 = 0.006, and the reference vector (RV) is −5 to −8‰ and for B) r1(σ_{ms}) = 0.15‰, ε^2 = 0.02, and RV is −1 to −4‰.

climatic scenarios.

The $\delta^{13}C$ range in the measured LACM-47129 enamel profile is 3.7‰ (−4.7 to −8.4‰), whereas m_{est_C} has a range of 8.1‰ (−2.7 to −10.8‰). $\delta^{18}O$ from enamel and m_{est_O} have similar ranges of 1.5‰ and 1.9‰, respectively. The entire profile (45 mm) appears to contain slightly more than one period of oscillation in carbon and oxygen. While it is tempting to suggest the profiles have the same periodicity, the record is not long enough to say this with confidence. Moreover, approximately half of the record was sampled from enamel within 25 mm of the cervix where changes in α, l_a, and possibly growth and maturation rates occur. Even with the limited profile length, dietary interpretations of the m_{est_C} and the enamel data yield two different results. With enamel data alone, one would infer a generally mixed C_3-C_4 diet throughout the year, ranging from ~40 to 65% C_4 vegetation based on a two end-member mixing model. The m_{est_C} values tell a different story. They indicate a greater range (20–80% C_4) and show a greater reliance on a single vegetation type (of up to ~80% C_3 or C_4) throughout the year. The data further suggest a larger seasonal change in vegetation than one would infer from the enamel data alone. Mammoths are thought to have been primarily grazers, and therefore, the data may indicate seasonal variation in grass type or conversely, a flexible diet that included C_3 browse and C_4 grasses. M_{est_C} and m_{est_O} from LACM-47129 highlight the potential utility of the model for longer profiles that encompass 2 or more years.

The IMNH-40368 enamel profiles exhibit a very small range of values over a ~55 mm interval from 92 to 36 mm that represents more than half of the time contained in the molar plate. In the interval from 25 mm to the cervix, the profiles show greater variability. Opacity of thin section IMNH-40368 under plane-polarized transmitted light throughout most of this interval suggests the region was still in the maturation phase

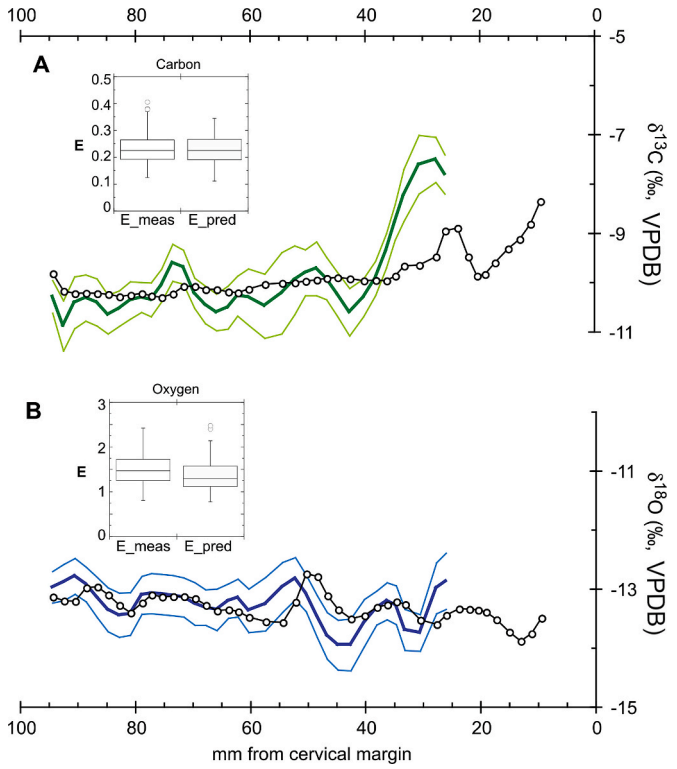

Fig. 14. Inverse model results for A) $\delta^{13}C$ and B) $\delta^{18}O$ from conventional sampling of mammoth molar IMNH-40368. Bold colored line is the mean m_{est} from 100 solutions ($\pm 1\sigma$) and circles are measured data. In both models $l_a = 30$ mm, $l_m = 60$ mm, openindx = 1, $r2(\sigma_{\Delta x}) = 0.5$ mm, and $r3(\sigma_{\Delta z}) = 0.5$ mm. For A) $r1(\sigma_{ms}) = 0.1‰$, $\varepsilon^2 = 0.005$, and the reference vector (RV) is −8 to −11‰ and for B) $r1(\sigma_{ms}) = 0.2‰$, $\varepsilon^2 = 0.05$, and RV is −11 to −14‰. Profile data from within 25 mm of the cervix, where growth rates show non-linear variation and enamel geometry changes, were omitted from the inversion.

(Fig. 6), whereby the higher organic content and smaller apatite crystal size may have made it more susceptible to diagenesis (c.f., bone or tooth dentin). This is also the region of the plate where appositional geometry changes dramatically. For these reasons, enamel profile data below 25 mm were excluded from the inverted data set, and are not discussed further here.

The $\delta^{13}C$ range in the enamel profile from 92 to 36 mm is 0.4‰ and the $\delta^{18}O$ range is 0.8‰. Model solutions over this same range for m_{est_C} and m_{est_O} are 1.2‰ and 1.5‰, respectively. Both m_{est} and enamel profiles indicate that throughout most of the period of record, the individual had an isotopically constant (C_3-dominated) diet and body water composition. Given that the fossil was found in or near lacustrine sediments, it is likely the mammoth relied on drinking water from a lake large enough to buffer variation in the $\delta^{18}O$ of the water throughout the year. Although the enamel profiles, especially carbon, are essentially constant, model solutions for both isotopes show in-phase, low amplitude, quasi-sinusoidal periodicity that could be interpreted as weak (and possibly annual) seasonal variability. This sort of tantalizing interpretation is tenuous and a rigorous test for a seasonal signal at the American Falls site would ideally include multiple enamel profiles from proboscideans and other coeval hypsodont taxa whose enamel mineralization and geometry is understood.

5. Discussion

5.1. Stable isotope turnover in elephants

The results from the M640 tusk profile provide a unique opportunity to evaluate the turnover time of carbon and oxygen in tusk dentin, and by extension elephant body water and blood bicarbonate. We focus on the body water turnover time and show that the half life, $t_{1/2}$, is on the order of one week. This result is similar to $t_{1/2}$ values for other large mammals, ranging from 3 to 13 days, that were compiled by Green et al. (2018b) and mostly come from an earlier study by Macfarlane et al. (1971). Aside from collecting breath samples before, during, and after the move from CA to UT to measure the isotope ratios of respired CO_2, which was not done with Misha, the tusk profile serves as the best record of turnover of carbon and oxygen in the body. Misha's tusk profile shows turnover of carbon and oxygen isotopes occurs at indistinguishable rates over a 293 μm interval. If the radial growth rate of ~19 μm/day is assumed, turnover occurs in 15 days, or if the growth rate is ~15 μm/day, as calculated from the date of the move from California to the date of death, then turnover is complete in 20 days. Thus, estimated turnover rates are 5–7%/day for carbon and oxygen in elephant blood bicarbonate and body water and support the assumption that elephant dentin undergoes minimal to no maturation based on histological studies (Boyde and Jones, 1972).

5.2. Comparison of sampling methods for intratooth profiles

Conventional drilling, micromilling, and laser ablation were used to generate isotope profiles from Misha_Rm3.5 in order to determine which method produces a profile that best resembles the primary input signal. Other considerations include sample preparation, time required to complete the sampling, and accessibility to necessary instrumentation. The magnitude of the isotopic shift associated with the move from each profile, expressed as Δδ, is given in Table 5. The isotopic shift in tusk profile M640 is also included in Table 5, and it is assumed to represent the primary input signal. A convenient way to evaluate the extent to which the enamel profiles are damped is to calculate the percent of the total amplitude (% $\Delta\delta_{tusk}$) they capture with respect to that observed in the tusk profile. For carbon, the micromill and conventional drilling methods both capture <50% of the true amplitude, whereas the laser captures 72%. Oxygen results show that conventional and laser methods both recover *ca.* 65% of the true amplitude and the micromill captures 44%. When m_{est} values are included in the comparison to the primary input signals, they perform the best of all methods, essentially capturing the true input signal, albeit slightly over-predicted at 110% of the true amplitude for both isotopes (Table 5). These data suggest that conventional sampling, which is the fastest and least destructive of the sampling methods explored here, coupled with inverse modeling, is the best method for producing isotope profiles that match the amplitude of the primary input signal. Adapting the existing model for sheep teeth

Table 5
Comparison of the magnitude of isotopic shift (Δδ) associated with the move from CA to UT by sampling method. The magnitude of the shift in the enamel is also shown as a % of the shift in the M640 tusk dentin profile, which is assumed to represent the primary input signal. Enamel maturation and sample geometry lead to damping of the full magnitude of the shift. Conv. = conventional, and "conv. + modeled" is the result of running the conventional data in the inversion model.

Sample ID	Sampling method	Δ $\delta^{13}C$ (‰)	%Δ $\delta^{13}C_{tusk}$	Δ $\delta^{18}O$ (‰)	%Δ $\delta^{18}O_{tusk}$
Enamel					
Misha_Rm3.5	micromill	−3.1	37%	−2.2	44%
Misha_Rm3.5	laser	−6.0	72%	−3.2	64%
Misha_Rm3.5	conv.	−4.0	48%	−3.4	68%
Misha_Rm3.5	conv. + model	−9.1	110%	−5.5	110%
Tusk dentin					
Misha_M640	micromill	−8.3	–	−5.0	–

developed by Green and colleagues to other mammal lineages or the Passey inverse model for additional lineages and tooth types are both promising next steps (Green et al., 2018a,b; Passey et al., 2005).

The laser profiles captured *ca.* 70% of the amplitude of the shift, but there are several limitations to this method. The laser system is best suited to samples on the order of millimeters, but can accommodate centimeter-scale samples, which makes analysis of proboscidean molar plates impossible unless they can be cut into small segments, as was done here. Furthermore, interpretation of $\delta^{18}O$ data is complicated by the inclusion of phosphate oxygen, and there is a paucity of labs that currently have LA-GC-IRMS systems ($n \approx 5$). The micromill is more widely available than the laser system, but the micromilled profile yielded lower amplitudes than the conventional method. A potential source of damping in the case of Misha_Rm3.5 is error in the angle at which mill paths are drilled. Minor variations from the true α angle when setting the mill paths, variability in α throughout the enamel profile, or undulation of the EDJ can all lead to mismatch between micromill paths and the true appositional surface. Micromilling of molar enamel differs from tusk dentin because in the latter case, second-order increments serve as a "road map" to keep mill paths parallel to growth increments, whereas with the former, one is left to mill paths by "dead reckoning" as increments in enamel are not visible in thick sections (Fig. 11).

5.3. Histological analyses

The histological data from molar thin sections contribute critical information to this study: they provide two ways to measure l_a and allow for measurement of α and DSR values, which enable calculations of CFT. A key finding from all three thin sections is that the angle of apposition, α, increases significantly within 25 mm of the cervix. This observation is in agreement with previous studies which have documented a similar increase in the appositional angle toward the cervix in caprine (Zazzo et al., 2012), suid (Yang et al., 2020), and proboscidean (Metcalfe and Longstaffe, 2014; Dirks et al., 2012) molars. It is also noteworthy that in fully mature plates, enamel thickness begins to decrease at 25–30 mm above the cervix (Fig. S11). Both the Misha and R37 molar profiles lacked tusk profile data corresponding to the lowest 25 mm of the studied plates because the corresponding portions of their tusks were not sampled. Without data to evaluate the behavior of the isotope profiles during this interval where mineralization geometry changes significantly, the most cautious recommendation is to avoid inverse modeling of isotope profile data from this interval until additional studies are done. The IMNH-40368 enamel profile was truncated at 25 mm above the cervix (Fig. 14), but the entire LACM-47129 profile was input into the model because only one-third of the profile was sampled below 25 mm.

5.4. Forward and inverse model parameters

The overall performance of the forward and inverse models for the Misha and R37 molar data is discussed here with an emphasis on evaluating the potential application to fossil proboscidean molars. For elephant molars, forward model parameters $f_i = 0.65$, $l_m = 70$ mm, and $l_a = 35$ mm (the shortest length) applied to the tusk profiles fit the measured enamel signal best; however, the intermediate l_a (45 mm) was used in inversions. In the Misha forward models (Fig. 9), the modeled enamel data show a better overall fit to the measured data after the move to Utah, but overall, both perform sufficiently well over the 3+ year period at reconstructing the amplitude and frequency recorded in the measured enamel profile.

A series of sensitivity tests on the three main parameters, f_i, l_a, and l_m was done in the inverse model with the Misha $\delta^{18}O$ profile (Fig. S16). The tests consisted of changing a single parameter at a time within a range of plausible values. For f_i, the values ranged from 0.25 to 0.75. The lower value of 0.25 was chosen because this value has been measured in teeth of several mammals (e.g., *Hippopotamus amphibius*, *Bos taurus*, *Bison bison*, *Equus* sp.) and has been suggested for a variety of other taxa including rodents (incisors) and ungulates. Results indicate the f_i value of 0.65 determined by micro-CT is accurate and relatively robust: values of 0.55 and 0.75 result in minor differences for the Misha $\delta^{18}O$ profile (Fig. S16). Thus, the differences observed between f_i values of inner enamel (0.65–0.7) versus those of other enamel (0.55–0.65) may not have a significant effect on inversion results. A difference of this magnitude in f_i (~0.10) would, however, have a larger effect if f_i were 0.25 as is the case for some mammal teeth. The results also show that an f_i value of 0.25 is not appropriate for elephant molars.

The maturation length was evaluated at lengths of 50, 75, and 100 mm, with f_i fixed at 0.65 and l_a at 45 mm, and shows very little change with different l_m lengths (Fig. S16). The small effect of changes in l_m is to be expected since ~65% of the signal is recorded in the secretory phase of enamel formation. Changes in l_m will have a greater damping effect for teeth with a lower f_i.

The model showed the greatest sensitivity to the parameter l_a (Fig. S16). In the case of elephant molars, where f_i is relatively high, the appositional length is responsible for a significant amount of time averaging, which increases with sampling depth z. Appositional lengths tested ranged from 20 to 100 mm and although the shortest length produced the best results, it is an unrealistic value for elephant molars based on multiple types of histological data presented here.

In summary, sensitivity tests on the Misha $\delta^{18}O$ profile suggest the f_i value determined in this study is accurate and exhibits low sensitivity to changes of *ca.* ± 0.1. There is little variation with changes in l_m, which is due to the relatively high f_i. The model is most sensitive to l_a because it imparts a significant damping effect on the primary input signal.

The large shift in the Misha $\delta^{18}O$ profile made it an obvious candidate for the sensitivity tests. It may be possible that the uniqueness of the profile, the one-way shift, may not be representative of seasonal (e.g., annual or biannual) changes in the primary input signal. Due to uncertainty in chronology and growth rates, there is still some uncertainty in matching of the profiles from the R37 molar and tusk. This precludes meaningful results from sensitivity tests on the R37 profiles, but generating profiles from adjacent molar plates or tusk dentin slabs would address this issue.

Both forward and inverse model results from Misha_Rm3.5 show regions of misfit to the measured profile. The misfit can be decomposed into offset in the y-axis (isotopic) or in the x-axis (temporal). Uncertainty in both variables warrants discussion because it may impart significant effects that could also be attributed to inadequate parameterization.

The principal source of isotopic uncertainty arises from the assumption that the tusk profile is representative of the primary input signal. The intratooth tusk dentin profiles from M640 (Figs. 8 and S12) convincingly show that tusk dentin is a high-fidelity recorder of stable isotope ratios at approximately weekly resolution, but do they record the full range of isotope variation? Comparison of the $\delta^{13}C$ of diet ($\delta^{13}C_{diet}$) based on R37 tail hair and tusk dentin during 2006 shows ranges that are very similar, (4.8 and 4.5‰, respectively; Uno et al., 2020). Yet when $\delta^{13}C_{diet}$ is calculated from tail hair data with the Reaction Progress Variable (RPV) model (Cerling et al., 2007), the modeled $\delta^{13}C_{diet}$ range for hair becomes 8.5‰, or nearly twice the range observed in the tusk dentin. An important caveat is that the 8.5‰ range in $\delta^{13}C_{diet}$ assumes the RPV model is correctly parameterized for elephants. The RPV parameters for turnover times and reservoir sizes are mathematically determined from experimental data collected on horses. Differences in body mass and physiology between the two taxa may result in different parameters for elephants, but to what extent we do not know. Nevertheless, the RPV model results indicate tusk dentin may underestimate the seasonal change in $\delta^{13}C_{diet}$. So while tusk profiles provide high-resolution isotopic records, the comparison of tusk dentin and hair $\delta^{13}C_{diet}$ records suggests that tusk dentin profiles may not fully represent the true primary input signal that is being sought or that the RPV model parameters could be improved for elephants.

Growth rate must be assigned to molars and tusks in order to convert isotope profiles from two different length domains into the time domain for comparison. Uno et al. (2013) and Uno et al. (inpress; Uno, 2012) show that bomb-curve ^{14}C dating or histological methods can be used to calculate tusk growth rates and the ^{14}C method is also applicable to proboscidean molars. In this study, we add histological analysis of molar thin sections as another method for determining growth rates in teeth. Measurement of perikymata is not applicable to elephant molars because they have a rugose enamel surface that usually obscures this feature, the time period in the increment is currently unknown, and they are eventually covered with cementum. Tusk and molar growth rates were determined using all methods available and although results of the histological and ^{14}C methods both converge on a radial growth rate of *ca.* 19 μm/day for Misha's tusk based on the M640 tusk slab, the isotope data indicate a growth rate of *ca.* 15 μm/day. Misha's ^{14}C-derived growth rate is based on data from along the entire length of the tusk, which may not be representative of the last 5 years of her life, as tusk growth rates can change throughout life (Fisher, 2008; Fisher et al., 2008). Reconciling the difference between the histological-based growth rate and the isotope-based growth rate is more difficult. It may be that the "weekly" value assumed is not 7.0 days, or varies between individuals. A shorter time period of about 5 days for second-order increments would bring the two growth rates into agreement.

Molar growth rates also show differences based on the method used. Uno et al. (2013) presented growth rates for six plates from two molars that ranged from 14 to 16 mm/year, and from one of these plates (TE-95_Rm3.7), a thin section was made in order to directly compare ^{14}C- and histologically-derived growth rates. The histological data from TE-95_Rm3.7 suggest a growth rate of about 22 mm/year. The histologically determined growth rates assume a constant DSR along the growth axis of the tooth, but this has not been verified. Nevertheless, the growth rates of the elephant molars are in good agreement with previous measurements on hypsodont proboscidean molars. Two studies on mammoth molars determined extension rates of ~14 mm/yr (Metcalfe and Longstaffe, 2012) and a range of 23 mm/yr near the occlusal surface to 12 mm/yr near the cervix (Dirks et al., 2012).

In summary, growth rates for tusks and teeth have been determined through a variety of methods and are in general agreement, but for the task at hand, which is to compare high-resolution isotope profiles from the two tissues on a temporal scale, variation in growth rates or uncertainties of even 10% in each tissue limit the ability to determine whether temporal offsets in the measured and modeled profiles are a result of imperfect model parameters or variations in growth rates. The observed misfit is likely due to some combination of both.

5.5. Application of the inverse model to fossil proboscidean molars

An important question to address is how meaningful are inversion results from fossil proboscidean molars? The mammoth profiles indicate that inverse models produce realistic estimated input signals, but there are considerations and caveats for other extinct proboscidean molars. Molar morphology of proboscideans outside of the subfamily Elephantinae is significantly different from that of the taxa evaluated in this study (e.g. Deinotheriidae or Gomphotheriidae), and therefore should not be evaluated with inverse methods using the parameters determined here. Even for species within the Elephantinae, similarity of tooth morphology to *L. africana* and *M. columbi* should be considered before applying the inverse model to enamel profiles. Model parameters f_i and l_m determined for African elephants are likely appropriate for fossil taxa within Elephantinae, but analysis by micro-CT or other methods for measuring density (e.g., phosphorus content, backscattered electron (BSE) microscopy) on well-preserved fossil specimens is recommended. It will also be necessary to determine crown formation times in fossil molars to transform profile data from length to time domains, keeping in mind that the CFT metric does not include the period of enamel maturation that occurs after crown formation is complete.

The 30 mm range of l_a values observed in African elephants is rather large, especially considering the sensitivity of inversion results to l_a (Fig. S16), and more developing molars of elephants should be characterized to determine the amount of variation that exists based on plate number (anterior to posterior), molar number, side of molar plate (e.g., mesial or distal), upper vs. lower dentition, and sex. These data will provide a framework for evaluating l_a values of fossil proboscidean plates, which must be determined histologically, or in the case of fossil molars that were developing when the animal died, this may be possible through measurement along the outer enamel surface.

Application of the inverse model with parameters determined in this study should be restricted to molars from Elephantinae. While this clade comprises only a small fraction of all lineages the order Proboscidea, taxa within the Elephantinae were the dominant proboscideans over the past *ca.* 6 Ma across most continents and therefore offer ample opportunity for studying the diet and life history of late Neogene proboscideans and the seasonality of vegetation and precipitation in their paleoenvironments. Careful morphological and histological study of molars from similar taxa such as *Primelephas* may extend the method beyond the genera studied here. These considerations apply to the general application of the inverse model to all mammalian teeth. Calculating an estimated input signal from an enamel profile using inverse methods is by definition an ill-posed problem as it is an underdetermined system. Thus, it is critical that the three key model parameters (f_i, l_a, and l_m) be determined on a case-by-case basis to the extent possible. Failure to do so increases the chance of producing erroneous and misleading model results.

5.6. Recommended profile and modeling scheme

The results of this study illustrate the potential use of inverse methods for recovering estimated primary input signals of dietary carbon or body water oxygen from intratooth profiles from hypsodont proboscidean (e.g., Elephantinae) molars. Here we recommend how one might pursue the use of inverse modeling of intratooth profiles in other mammalian teeth. The most important step is generating a robust forward model, which requires characterizing the parameters f_i, l_a, and l_m. This entails spatial analysis of enamel density to determine f_i and l_m, which in this study was done by micro-CT, but other methods such as measuring phosphorus content or using BSE microscopy are also available. Histological analysis via thin section is important for establishing growth rates and also provides a means for determining l_a.

Misha provided a unique case for testing the forward model because an intratooth profile from her tusk was available to serve as a primary input signal. Experiments on small mammals where a diet or water switch can be done are invaluable for developing and testing forward models (Green et al., 2017; Passey et al., 2005; Podlesak et al., 2008; Zazzo et al., 2010), but not entirely necessary (cf., Passey and Cerling, 2002). For larger animals, translocations between zoos or parks around the country can serve as unintended diet and water switches, as was the case with Misha. Collaborating with the Hogle Zoo in Salt Lake City has provided (and continues to provide) amazing opportunities to study isotope systematics in animal tissues and breath.

With regard to sampling protocols for enamel profiles, these will vary by tooth size, model parameters, and the frequency of the primary input signal (if known). For elephant molars, which grow ~15–22 mm/year, sampling every 2–3 mm was sufficient. In the case of East African elephants, where biannual rains lead to changes in the $\delta^{13}C$ of diet and the $\delta^{18}O$ of body water on timescales of 3–4 months, 2 mm represents a minimum sampling interval. Variation in growth rate must also be characterized on a relevant temporal scale. The model assumes linear growth and deviations from this will impart temporal error on model results and subsequent interpretations.

When conventionally drilling profiles, it is not critical to keep the sampling interval (Δx) and depth (Δz) constant since each of these variables is input with the corresponding d value (See Supplementary

Information) into the model. These parameters ultimately affect uncertainty in the model solutions, so it is critical to minimize Δx and Δz uncertainty. This can be accomplished through careful measurement after a profile is drilled using either a micrometer or via digital measurement from a scanned image of the molar profile. We found the latter method to be faster, and scanning also leaves you with a digital image of the profile. Finally, as discussed previously, in the lower portion of molar plates, l_a decreases as α increases. This occurs where the enamel thickness begins to decrease rapidly (Fig. S11). This change in the geometry of the appositional surface is not accounted for in the models used here, and profile samples from this interval should not be included in model input unless the model is adapted to account for this. This may be problematic for isotope profiles in smaller teeth. For example, Zazzo et al. (2012) found α increases in sheep teeth around 20 mm above the cervix, but since sheep molar crowns are only 40–50 mm in length, this means only 50–60% of the profile can be used in the inverse model. Adjustment to the model that accounts for changes in l_a as a function of length may permit inversion of profile data from the entire crown length, which would benefit those working on shorter molar crowns or well-worn proboscidean molar plates.

6. Conclusions

This study extends the use of the inverse model developed by Passey et al. (2005) for reconstructing the estimated primary input signal for continuously growing teeth to molars of proboscideans in Elephantinae. Using coeval tusk and enamel profiles from a translocated zoo elephant, we evaluated how well the inverse model could reconstruct the primary input signal from the enamel profile. Inverted conventionally sampled intratooth profiles have $\delta^{13}C$ and $\delta^{18}O$ amplitudes that are within 10% of tusk values, which were assumed to represent the primary input signal. Profiles generated by micromilling and laser ablation methods—both differing in sample orientation from the conventional method—yielded amplitudes ranging from 32 to 72% of the tusk amplitudes. Inversion results from conventionally drilled profiles successfully reconstruct the dominant structural features of the primary ($\delta^{13}C$ or $\delta^{18}O$) input signal, although some blurring still occurs. The structure of both the raw and inverted conventionally drilled profiles more closely resembles that of the tusk profile than the micromill and laser ablation profiles. The results demonstrate that the inverse model produces estimated primary input signals that more accurately reflect the true primary input signal than high-resolution sampling methods such as micromill or laser ablation scans.

Inversion of a molar profile from R37 suggests the record of seasonal diet change associated with the biannual rains in Kenya is preserved in elephant enamel, but uncertainty in the time interval represented by this profile precludes confident temporal placement and direct comparison to tusk profile data from R37. Inversion of a mammoth molar profile from a late Pleistocene site in southern coastal California indicates a highly variable seasonal diet that ranged from 28 to 82% C_4 vegetation. Inversion of a seemingly flat molar profile from a late Pleistocene site in Idaho produced estimated primary input signals that suggest weak seasonality in diet and water.

The ability of the inverse model to reliably reconstruct estimated primary input signals hinges upon development of a robust forward model that accurately describes enamel formation and geometry. To this end, histological and micro-CT methods were employed to characterize forward model parameters f_i, l_a, and l_m. Elephant molar f_i is 65 ± 2%FD, which is about 2.5 higher than has been observed in other mammalian teeth. Elephant molar l_m is 70 ± 5 mm, which is similar but slightly longer than that measured in hippopotamus canines, and l_a measurements based on three methods range from about 35 to 55 mm. Future work should be directed toward determining the optimal method for measuring l_a, and characterizing the variability among extant (and fossil) proboscideans. The results from the sensitivity test further demonstrate the significance of the parameter l_a in enamel formation.

Histological data suggest the CFT for elephant plates of first through third molars (M1 to M3) is 4.8–6 years based on measured appositional angles (α) and a constant DSR of 3 μm/day. This implies growth rates of 20–22 mm/year. ^{14}C-based growth rates are lower than those determined using histological methods, ranging from 13 to 16 mm/year. The histological method yields a CFT that does not include the time required for enamel maturation after crown extension is complete, whereas the ^{14}C method does include maturation. Mammoth molar growth rates are not constant over the entire CFT, but they average ~11 years assuming a constant DSR of 3.5 μm/day. This should be considered when applying the inverse model to profiles greater than approximately 10 cm in length, where effects of a variable growth rate become pronounced. Histological analyses reveal a change in appositional angle near the cervical margin, coinciding with a marked decrease in enamel thickness that will affect inverse model results. Therefore, enamel profile data from this region should not be included in the inverse model unless the forward and inverse models are adapted to account for this. Application of the inverse model to teeth from the proboscidean subfamily Elephantinae provides a new proxy for estimating the timing and magnitude of seasonality in ancient ecosystems spanning the last 6 million years and most continents.

Data availability

Data are available as Supplementary Tables in Excel format and online through the Interdisciplinary Earth Data Alliance (www.iedadata.org).

Declaration of competing interest

The authors declare that they have no known competing financial interests or personal relationships that could have appeared to influence the work reported in this paper.

Acknowledgements

We thank the Office of the President of the Republic of Kenya, the Kenya Wildlife Service, the Samburu and Buffalo Springs County Councils, and Utah's Hogle Zoo for permission to conduct this research. We thank elephant keeper Doug Thompkins at Utah's Hogle Zoo; David Daballen, Daniel Lentipo, and Chris Leadismo at Save The Elephants for sample collection; Scott Beld, Dan Davis, and Jared Singer for assistance with sample preparation, photomicroscopy, and isotope analyses; Adam Rountrey for furnishing a copy of the ImageJ plug-in (IncMeas v1.2) used to measure growth increments; CL Lin and Ching Hoa Hsieh for assistance with micro-CT work at the University of Utah; and Fernando Medina for access to and assistance with the pycnometer in Jan Miller's laboratory. We thank John M. Harris at the Los Angeles County Museum and Mary Thompson at the Idaho Museum of Natural History for information on fossil proboscidean material. We also thank the two anonymous reviewers whose critical comments significantly improved this very long manuscript. Research was supported by National Science Foundation grants EAR-0819611 and BCS-0621542, a University of Utah Graduate Research Fellowship, and the Department of Geology and Geophysics' Graduate Research Fund. This work was carried out under CITES permits US831854/9, 02US053837/9, and 07US159997/9. This is Lamont-Doherty Earth Observatory contribution #8434.

Appendix A. Supplementary data

Supplementary data to this article can be found online at https://doi.org/10.1016/j.quaint.2020.06.030.

References

Ayliffe, L., Chivas, A., Leakey, M., 1994. The retention of primary oxygen isotope compositions of fossil elephant skeletal phosphate. Geochem. Cosmochim. Acta 58, 5291–5298.
Balasse, M., 2002. Reconstructing dietary and environmental history from enamel isotopic analysis: time resolution of intra-tooth sequential sampling. Int. J. Osteoarchaeol. 12, 155–165.
Balasse, M., 2003. Potential biases in sampling design and interpretation of intra-tooth isotope analysis. Int. J. Osteoarchaeol. 13, 3–10.
Balasse, M., Ambrose, S.H., Smith, A.B., Price, T.D., 2002. The seasonal mobility model for prehistoric herders in the south-western Cape of South Africa assessed by isotopic analysis of sheep tooth enamel. J. Archaeol. Sci. 29, 917–932.
Balasse, M., Smith, A.B., Ambrose, S.H., Leigh, S.R., 2003. Determining sheep birth seasonality by analysis of tooth enamel oxygen isotope ratios: the Late Stone Age site of Kasteelberg (South Africa). J. Archaeol. Sci. 30, 205–215.
Blumenthal, S.A., Cerling, T.E., Chritz, K.L., Bromage, T.G., Kozdon, R., Valley, J.W., 2014. Stable isotope time-series in mammalian teeth: in situ $\delta^{18}O$ from the innermost enamel layer. Geochem. Cosmochim. Acta 124, 223–236.
Blumenthal, S.A., Cerling, T.E., Smiley, T.M., Badgley, C.E., Plummer, T.W., 2019. Isotopic records of climate seasonality in equid teeth. Geochem. Cosmochim. Acta 260, 329–348.
Boyde, A., Jones, S.J., 1972. Scanning electron microscopic studies of the formation of mineralized tissues. In: Slavkin, H.C., Bavetta, L.A. (Eds.), Developmental Aspects of Oral Biology. Academic Press, New York, pp. 263–274.
Cerling, T.E., Ayliffe, L.K., Dearing, M.D., Ehleringer, J.R., Passey, B.H., Podlesak, D.W., Torregrossa, A.M., West, A.G., 2007. Determining biological tissue turnover using stable isotopes: the reaction progress variable. Oecologia 151, 175–189.
Dettman, D.L., Kohn, M.J., Quade, J., Ryerson, F., Ojha, T.P., Hamidullah, S., 2001. Seasonal stable isotope evidence for a strong Asian monsoon throughout the past 10.7 my. Geology 29, 31.
Dirks, W., Bromage, T.G., Agenbroad, L.D., 2012. The duration and rate of molar plate formation in *Palaeoloxodon cypriotes* and *Mammuthus columbi* from dental histology. Quat. Int. 255, 79–85.
Elliott, J.C., 2002. Calcium phosphate biominerals. In: Kohn, M.J., Rakovan, J., Hughes, J. (Eds.), Phosphates- Geochemical, Geobiological, and Materials Importance. The Mineralogical Society of America, Chantilly, pp. 427–453.
Fisher, D.C., 2008. Taphonomy and paleobiology of the hyde park mastodon. Palaeontogr. Am. 61, 197–289.
Fisher, D.C., Beld, S.G., Rountrey, A.N., Allmon, W.D., Nester, P.L., 2008. Tusk record of the North Java mastodon. Palaeontogr. Am. 61, 417–463.
Fisher, D.C., Fox, D.L., 2007. Season of death of the dent mammoths. In: Brunswig, R.H., Pitblado, B.L. (Eds.), From the Dent Prairie to the Peaks of the Rockies: Recent Paleoindian Research in Colorado. University of Colorado Press, Boulder, pp. 123–153.
Frémondeau, D., Cucchi, T., Casabianca, F., Ughetto-Monfrin, J., Horard Herbin, M., Balasse, M., 2012. Seasonality of birth and diet of pigs from stable isotope analyses of tooth enamel ($\delta^{18}O$, $\delta^{13}C$): a modern reference data set from Corsica, France. J. Archaeol. Sci.
Fricke, H.C., Clyde, W.C., O'Neil, J.R., 1998. Intra-tooth variations in $\delta^{18}O$ (PO_4) of mammalian tooth enamel as a record of seasonal variations in continental climate variables. Geochem. Cosmochim. Acta 62, 1839–1850.
Fricke, H.C., O'Neil, J.R., 1996. Inter-and intra-tooth variation in the oxygen isotope composition of mammalian tooth enamel phosphate: implications for palaeoclimatological and palaeobiological research. Palaeogeogr. Palaeoclimatol. Palaeoecol. 126, 91–99.
Green, D.R., Green, G.M., Colman, A.S., Bidlack, F.B., Tafforeau, P., Smith, T.M., 2017. Synchrotron imaging and Markov chain Monte Carlo reveal tooth mineralization patterns. PloS One 12, e0186391.
Green, D.R., Smith, T.M., Green, G.M., Bidlack, F.B., Tafforeau, P., Colman, A.S., 2018a. Quantitative reconstruction of seasonality from stable isotopes in teeth. Geochem. Cosmochim. Acta 235, 483–504.
Green, D.R., Olack, G., Colman, A.S., 2018b. Determinants of blood water $\delta^{18}O$ variation in a population of experimental sheep: implications for paleoclimate reconstruction. Chem. Geol. 485, 32–43.
Hiller, C.R., Robinson, C., Weatherell, J.A., 1975. Variations in the composition of developing rat incisor enamel. Calcif. Tissue Int. 18, 1–12.
Hoppe, K.A., Stover, S.M., Pascoe, J.R., Amundson, R., 2004. Tooth enamel biomineralization in extant horses: implications for isotopic microsampling. Palaeogeogr. Palaeoclimatol. Palaeoecol. 206, 355–365.
Koch, P.L., Fisher, D.C., Dettman, D., 1989. Oxygen isotope variation in the tusks of extinct proboscideans: a measure of season of death and seasonality. Geology 17, 515–519.
Koch, P.L., Hoppe, K.A., Webb, S.D., 1998. The isotopic ecology of late Pleistocene mammals in North America: Part 1. Florida. Chem. Geol. 152, 119–138.
Kohn, M.J., Miselis, J.L., Fremd, T.J., 2002. Oxygen isotope evidence for progressive uplift of the Cascade Range, Oregon. Earth Planet Sci. Lett. 204, 151–165.
Laws, R., 1966. Age criteria for the African elephant, Loxodonta a. africana. East Afr. Wildl. J. 4, 1–37.
Lee, P.C., Sayialel, S., Lindsay, W.K., Moss, C.J., 2012. African elephant age determination from teeth: validation from known individuals. Afr. J. Ecol. 50, 9–20.
Lee-Thorp, J.A., dan der Merwe, N.J., 1987. Carbon isotope analysis of fossil bone apatite. South Afr. J. Sci. 83, 712–715.
Macfarlane, W., Howard, B., Haines, H., Kennedy, P., Sharpe, C., 1971. Hierarchy of water and energy turnover of desert mammals. Nature 234, 483–484.
Metcalfe, J.Z., Longstaffe, F.J., Ballenger, J.A.M., Haynes Jr., C.V., 2011. Isotopic paleoecology of Clovis mammoths from Arizona. Proc. Natl. Acad. Sci. Unit. States Am. 108, 17916–17920.
Metcalfe, J.Z., Longstaffe, F.J., 2012. Mammoth tooth enamel growth rates inferred from stable isotope analysis and histology. Quat. Res. 77, 424–432.
Metcalfe, J.Z., Longstaffe, F.J., 2014. Environmental change and seasonal behavior of mastodons in the Great Lakes region inferred from stable isotope analysis. Quat. Res. 82, 366–377.
Miller, W.E., 1971. Pleistocene vertebrates of the Los Angeles basin and vicinity (exclusive of Rancho La Brea). Bull. Los Angel. Cty. Mus. Nat. Hist. Sci. 10, 124.
Moss-Salentijn, L., Moss, M., Yuan, M.S., 1997. The ontogeny of mammalian enamel. In: Von Koenigswald, W., Sander, P. (Eds.), Tooth Enamel Microstructure. AA Balkema, Rotterdam, pp. 5–30.
Passey, B.H., Cerling, T.E., 2002. Tooth enamel mineralization in ungulates; implications for recovering a primary isotopic time-series. Geochem. Cosmochim. Acta 66, 3225–3234.
Passey, B.H., Cerling, T.E., 2004. Response to the comment by MJ Kohn on "Tooth enamel mineralization in ungulates: implications for recovering a primary isotopic time-series" by BH Passey and TE Cerling (2002). Geochem. Cosmochim. Acta 68, 407–410.
Passey, B.H., Cerling, T.E., 2006. In situ stable isotope analysis ($\delta^{13}C$, $\delta^{18}O$) of very small teeth using laser ablation GC/IRMS. Chem. Geol. 235, 238–249.
Passey, B.H., Cerling, T.E., Perkins, M.E., Voorhies, M.R., Harris, J.M., Tucker, S.T., 2002. Environmental change in the Great Plains; an isotopic record from fossil horses. J. Geol. 110, 123–140.
Passey, B.H., Cerling, T.E., Schuster, G.T., Robinson, T.F., Roeder, B.L., Krueger, S.K., 2005. Inverse methods for estimating primary input signals from time-averaged isotope profiles. Geochem. Cosmochim. Acta 69, 4101–4116.
Pinsof, J.D., 1992. The Late Pleistocene Vertebrate Fauna from the American Falls Area, Southeastern Idaho. Idaho State University.
Podlesak, D.W., Torregrossa, A.-M., Ehleringer, J.R., Dearing, M.D., Passey, B.H., Cerling, T.E., 2008. Turnover of oxygen and hydrogen isotopes in the body water, CO_2, hair, and enamel of a small mammal. Geochem. Cosmochim. Acta 72, 19–35.
Rountrey, A.N., 2009. Life Histories of Juvenile Woolly Mammoths from Siberia: Stable Isotope and Elemental Analyses of Tooth Dentin. University of Michigan, Ann Arbor, MI, USA.
Rountrey, A.N., Fisher, D.C., Tikhonov, A.N., Kosintsev, P.A., Lazarev, P.A., Boeskorov, G., Buigues, B., 2012. Early tooth development, gestation, and season of birth in mammoths. Quat. Int. 255, 196–205.
Rountrey, A.N., Fisher, D.C., Vartanyan, S., Fox, D.L., 2007. Carbon and nitrogen isotope analyses of a juvenile woolly mammoth tusk: evidence of weaning. Quat. Int. 169, 166–173.
Schoeninger, M.J., DeNiro, M.J., 1982. Carbon Isotope Ratios of Apatite from Fossil Bone Cannot Be Used to Reconstruct Diets of Animals.
Scott, W., Pierce, K., Bradbury, J.P., Forester, R., 1982. Revised Quaternary stratigraphy and chronology in the American Falls area, southeastern Idaho. Cenozoic Geol. Idaho: Idaho Bur. Mine Geol. Bull. 26, 581–595.
Suga, S., 1982. Progressive mineralization pattern of developing enamel during the maturation stage. J. Dent. Res. 1532.
Suga, S., 1989. Enamel hypomineralization viewed from the pattern of progressive mineralization of human and monkey developing enamel. Adv. Dent. Res. 3, 188–198.
Tafforeau, P., Bentaleb, I., Jaeger, J.J., Martin, C., 2007. Nature of laminations and mineralization in rhinoceros enamel using histology and X-ray synchrotron microtomography: potential implications for palaeoenvironmental isotopic studies. Palaeogeogr. Palaeoclimatol. Palaeoecol. 246, 206–227.
Tornero, C., Aguilera, M., Ferrio, J.P., Arcusa, H., Moreno-García, M., Garcia-Reig, S., Rojo-Guerra, M., 2018. Vertical sheep mobility along the altitudinal gradient through stable isotope analyses in tooth molar bioapatite, meteoric water and pastures: a reference from the Ebro valley to the Central Pyrenees. Quat. Int. 484, 94–106.
Trayler, R.B., Kohn, M.J., 2017. Tooth enamel maturation reequilibrates oxygen isotope compositions and supports simple sampling methods. Geochem. Cosmochim. Acta 198, 32–47.
Uno, K.T., 2012. Advances in Terrestrial Paleoecology from Intratooth Stable Isotope Profiles in Tooth Enamel and Tusk Dentin, Geology and Geophysics. University of Utah, Salt Lake City, UT, p. 307.
Uno, K.T., Bibi, F., 2020. Stable isotope paleoecology of the late miocene baynunah formation, Abu Dhabi, United Arab Emirates. In: Bibi, F., Kraatz, B., Beech, M. (Eds.), Sands of Time. Springer in press.
Uno, K.T., Quade, J., Fisher, D.C., Wittemyer, G., Douglas-Hamilton, I., Andanje, S., Omondi, P., Litoroh, M., Cerling, T.E., 2013. Bomb-curve radiocarbon measurement of recent biologic tissues and applications to wildlife forensics and stable isotope (paleo) ecology. Proc. Natl. Acad. Sci. Unit. States Am. 110, 11736–11741.
Uno, K.T., Fisher, D.C., Schuster, G.T., Wittemyer, G., Douglas-Hamilton, I., Omondi, P., Litoroh, M., Cerling, T.E., 2020. High-resolution stable isotope profiles of modern elephant (*Loxodonta africana*) tusk dentin and tail hair from Kenya: implications for identifying seasonal variability in climate, ecology, and diet in ancient proboscideans. Palaeogeogr. Palaeoclimatol. Palaeoecol. https://doi.org/10.1016/j.palaeo.2020.109962.
Wang, Y., Cerling, T.E., 1994. A model of fossil tooth and bone diagenesis: implications for paleodiet reconstruction from stable isotopes. Palaeogeogr. Palaeoclimatol. Palaeoecol. 107, 281–289.
Weatherell, J., Robinson, C., Hallsworth, A., 1974. Variations in the chemical composition of human enamel. J. Dent. Res. 53, 180–192.

Widga, C., Hodgins, G., Kolis, K., Lengyel, S., Saunders, J., Walker, J.D., Wanamaker, A. D., 2020. Multi-scalar Approaches to stable isotope ecology of late Quaternary Proboscideans in the Midcontinent. bioRxiv. https://doi.org/10.1101/2020.01.08.896647.

Wittemyer, G., 2001. The elephant population of Samburu and Buffalo Springs national reserves, Kenya. Afr. J. Ecol. 39, 357–365.

Wittemyer, G., Getz, W.M., 2007. Hierarchical dominance structure and social organization in African elephants, Loxodonta africana. Anim. Behav. 73, 671–681.

Yang, D., Uno, K.T., Souron, A., McGrath, K., Pubert, E., Cerling, T.E., 2020. Intra-tooth stable isotope variations in warthog canines and third molars: implications for paleoenvironmental reconstruction. Chem. Geol. https://doi.org/10.1016/j.chemgeo.2020.119799.

Zazzo, A., Balasse, M., Passey, B., Moloney, A., Monahan, F., Schmidt, O., 2010. The isotope record of short-and long-term dietary changes in sheep tooth enamel: implications for quantitative reconstruction of paleodiets. Geochem. Cosmochim. Acta 74, 3571–3586.

Zazzo, A., Balasse, M., Patterson, W.P., 2005. High-resolution $d^{13}C$ intratooth profiles in bovine enamel: implications for mineralization pattern and isotopic attenuation. Geochem. Cosmochim. Acta 69, 3631–3642.

Zazzo, A., Bendrey, R., Vella, D., Moloney, A., Monahan, F., Schmidt, O., 2012. A refined sampling strategy for intra-tooth stable isotope analysis of mammalian enamel. Geochem. Cosmochim. Acta.